AD-A184 191 CORROSION BEHAVIOR OF P/M MECHANICALLY ALLOYED IN-90521 1/1
AN ELECTRO-CHEMIC (U) NAVAL SURFACE WEAPONS CENTER
SILVER SPRING MD P A STONE ET AL 01 DEC 86
UNCLASSIFIED NSWC/TR-86-412 F/G 11/6 NL

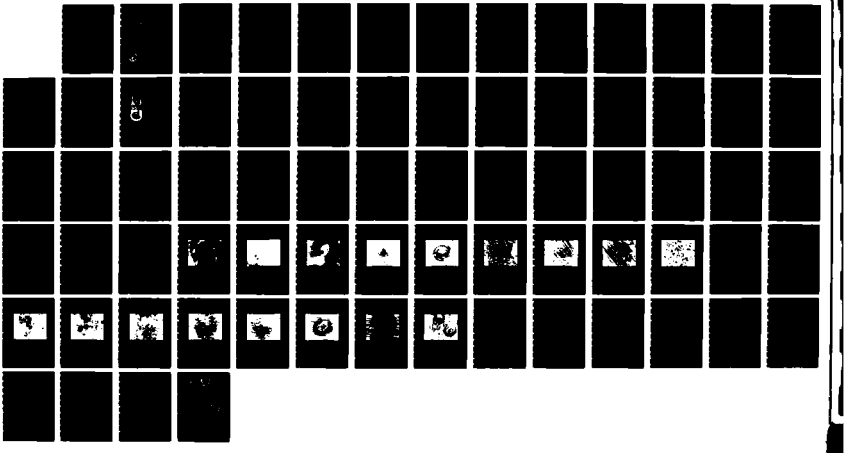

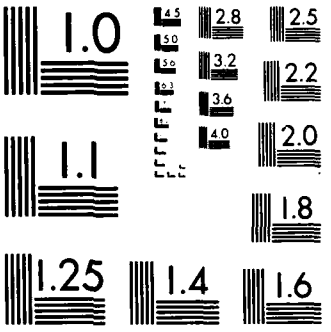

MICROCOPY RESOLUTION TEST CHART
NATIONAL BUREAU OF STANDARDS-1963-A

NSWC TR 86-412

CORROSION BEHAVIOR OF P/M MECHANICALLY ALLOYED IN-9052.I, AN ELECTRO-CHEMICAL INVESTIGATION

BY P. A. STONE J. F. McINTYRE R. K. GARRETT

RESEARCH AND TECHNOLOGY DEPARTMENT

1 DECEMBER 1986

Approved for public release; distribution is unlimited.

NAVAL SURFACE WEAPONS CENTER

Dahlgren, Virginia 22448-5000 • Silver Spring, Maryland 20903-5000

UNCLASSIFIED

SECURITY CLASSIFICATION OF THIS PAGE

ADA184191

REPORT DOCUMENTATION PAGE

1a. REPORT SECURITY CLASSIFICATION UNCLASSIFIED	1b. RESTRICTIVE MARKINGS
2a. SECURITY CLASSIFICATION AUTHORITY	3 DISTRIBUTION / AVAILABILITY OF REPORT Approved for public release; distribution is unlimited.
2b. DECLASSIFICATION / DOWNGRADING SCHEDULE	
4 PERFORMING ORGANIZATION REPORT NUMBER(S)	5. MONITORING ORGANIZATION REPORT NUMBER(S)
6a. NAME OF PERFORMING ORGANIZATION Naval Surface Weapons Center 6b OFFICE SYMBOL (*If applicable*) R33	7a. NAME OF MONITORING ORGANIZATION
6c. ADDRESS (*City, State, and ZIP Code*) 10901 New Hampshire Avenue Silver Spring, MD 20903-5000	7b. ADDRESS (*City, State, and ZIP Code*)
8a. NAME OF FUNDING / SPONSORING ORGANIZATION 8b. OFFICE SYMBOL (*If applicable*)	9. PROCUREMENT INSTRUMENT IDENTIFICATION NUMBER
8c. ADDRESS (*City, State, and ZIP Code*)	10 SOURCE OF FUNDING NUMBERS PROGRAM ELEMENT NO / PROJECT NO / TASK NO. / WORK UNIT ACCESSION NO

11 TITLE (*Include Security Classification*)
Corrosion Behavior of P/M Mechanically Alloyed IN-9052.I, An Electro-Chemical Investigation (U)

12 PERSONAL AUTHOR(S)
Stone, P. A., McIntyre, J. F., and Garrett, R. K.

13a. TYPE OF REPORT	13b TIME COVERED	14 DATE OF REPORT (*Year, Month, Day*)	15 PAGE COUNT
Technical Review	FROM _____ TO _____	86/12/1	72

16 SUPPLEMENTARY NOTATION

17 COSATI CODES			18. SUBJECT TERMS (*Continue on reverse if necessary and identify by block number*)
FIELD	GROUP	SUB-GROUP	Mechanical Alloying, Potentiodynamic Pitting, Polarization Resistance, Scanning Electron Microscopy
11	06	01	

19 ABSTRACT (*Continue on reverse if necessary and identify by block number*)

The corrosion behavior of P/M mechanically alloyed IN-9052 is compared to AA-6061-T6. Electrochemical techniques are used to study these alloys exposed to 3.5% NaCl. Scanning electron microscopy is used to characterize the morphology of freely corroding samples. A mechanism for pit initiation on IN-9052 is proposed.

20 DISTRIBUTION / AVAILABILITY OF ABSTRACT	21. ABSTRACT SECURITY CLASSIFICATION
☐ UNCLASSIFIED/UNLIMITED ☒ SAME AS RPT ☐ DTIC USERS	UNCLASSIFIED
22a NAME OF RESPONSIBLE INDIVIDUAL J. F. McIntyre	22b TELEPHONE (*Include Area Code*) (202) 394-4115 22c OFFICE SYMBOL R33

DD FORM 1473, 84 MAR 83 APR edition may be used until exhausted
All other editions are obsolete

SECURITY CLASSIFICATION OF THIS PAGE
UNCLASSIFIED

FOREWORD

Aluminum alloys combine high corrosion resistance to marine environments and high strength for use in advanced Naval weapons. Corrosion resistance is needed to reduce life-cycle costs while enhanced mechanical properties are needed to enable designers to produce lighter and stronger structures. INCO-9052, a mechanically alloyed P/M material, is a new aluminum alloy that shows great promise for torpedo and mine hull applications. The corrosion behavior and mechanical properties of INCO-9052 are being evaluated to establish a database. Such a database will assist in the transition of this alloy from experimental status to ordnance applications. This report summarizes some preliminary corrosion data on INCO-9052 using electrochemical techniques and scanning electron microscopy. This research was funded by the Materials Block Program.

The authors would like to express their sincere gratitude for the assistance of Dr. Marriner Norr (R34) for obtaining the SEM photographs and for the technical assistance provide by Kerry Woodfield (U32) and Scott Hoover (R32).

Approved by:

Jack R. Dixon, Head
Materials Division

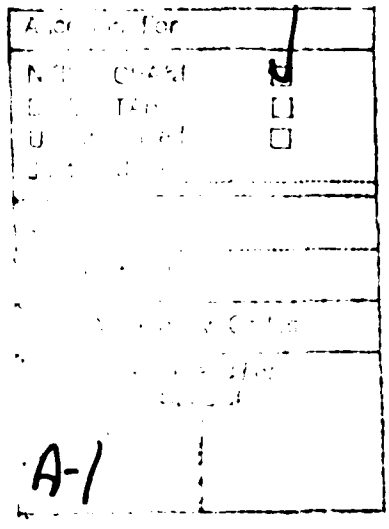

CONTENTS

ILLUSTRATIONS

ILLUSTRATIONS (cont)

ILLUSTRATIONS (cont)

TABLES

CHAPTER 1

INTRODUCTION

IN-9052, a powder/metallurgy mechanically alloyed aluminum alloy, is being evaluated as a possible replacement for AA-6061-T6 for underwater ordnance applications. Preliminary research indicates that IN-9052 has better corrosion resistance and mechanical properties than AA-6061-T6. Currently, it is proposed to replace AA-6061-T6 with IN-9052 in the MK 50 torpedo warhead hull section. The driving force for the proposed material change is a potential reduction in life-cycle costs; in the past, severe pitting of AA-6061 in the MK 50 torpedo has resulted in high maintenance costs.

This report is a first in a series of materials characterization studies on IN-9052. In this study, the corrosion behavior of IN-9052 has been investigated using electrochemical laboratory techniques.

CHAPTER 2

BACKGROUND

The anticipated benefits of using IN-9052 arise from its unique microstructure. IN-9052 is a mechanically alloyed powder metallurgy material with a composition of 4.0% Mg, 1.1% C, and 0.8% O with the balance Al, and compositionally similar to AA-5083. The constituents in powder form are alloyed by mechanically mixing and impacting with steel balls, thus, producing an alloy through repeated fracturing and cold-welding. Details of this process are given elsewhere.[1-3] This alloying process produces an alloy with a very fine grain structure with homogeneously dispersed carbides and oxides. These carbides and oxide particles (100-300 µA particle size) help to stabilize the submicron grain size. The total amount of dispersoid is about 2-4% by volume and better properties are possible because of these fine dispersoids;[3] for example, tensile tests show that yield strength, ultimate yield strength, and elongation are improved for IN-9052 compared to AA-6061. See Table 1.

The corrosion behavior of metals/alloys is strongly influenced by a large number of chemical and physical variables. Chemical influences involve the interaction of the material with its environment. Physical effects on corrosion behavior include: temperature, agitation, pressure, and presence of stray-currents. Another physical effect, not related to the environment, is associated with alloy composition and microstructure. Microstructure is affected by variables such as, alloying constituents, heat treatments, and fabrication history. The size and composition of the grain in an alloy can strongly affect corrosion behavior. For example, it is well established that corrosion occurs more easily at grain boundaries, slip dislocations, and other defects because the number of bonds to an atom are fewer and packing is more irregular.[4,5] The homogeneous distribution of fine despersoids in IN-9052 might ultimately lead to a more defect-free structure because dislocation formation is significantly reduced. In addition to the influence of the structure of the grain, the composition of grains and grain boundary regions can determine the susceptibility of an alloy to corrosion. For example, during heat treatment of stainless steels the presence of carbon causes the formation of chromium carbides in the grain boundary region, thus, depleting this area of free chromium and leading to preferential corrosion along grain

TABLE 1. MECHANICAL PROPERTIES OF IN-9052 AND AA-6061

Alloy	Tension Yield (ksi)	Tension UTS (ksi)	Elongation	Compression Yield (ksi)
AA-6061	40	45	12%	45
IN-9052	45	62	10%	55

boundaries, i.e., intergranular corrosion. Because IN-9052 has no recognizable grain structure, corrosion resistance is expected to be improved and grain structure effects should be negligible.

Thermodynamically, aluminum and its alloys are highly reactive and should corrode easily; however, as a result of this reactivity a protective oxide film is formed which imparts good corrosion resistance. Because of the highly protective nature of this oxide, aluminum alloys are susceptible to localized attack at weak spots, defects, or damaged areas in the oxide layer. An alloy with well developed grain structures, inherently, may have more defects in the oxide structure, thus, providing sites for localized attack. On the other hand, the highly strained-high energy F.C.C. crystal lattice of IN-9052 with its low angle boundaries inherently results in less mismatch between crystallographic planes. This inherent reduction in the mismatch between crystallographic planes may lead to the formation of a more defect-free surface oxide. An oxide with fewer defect sites would be expected to exhibit better corrosion resistance.

To date, only a small number of investigations have provided corrosion data for mechanically alloyed aluminum alloys.[6,7] A study by Erich and Donachie[6] gave corrosion rates of 0.1 and 12 MDD (milligrams per decimeter per day) for IN-9052 and IN-9021 exposed to alternate immersion in 3.5% NaCl; in comparison, AA-7075-T73 similarly tested gave a corrosion rate of 19 MDD; in this same study, exfoliation tests revealed that IN-9052 and IN-9021 had better resistance when compared to AA-7075-T73 and it was also determined that the stress corrosion cracking behavior of IN-9052 and IN-9021 was superior to that of AA-7075-T73. Shaw[7] studied the corrosion behavior of IN-9021-T452 exposed to 3.5% NaCl and gave corrosion rates of 8.8-23 MPY (mili-inches per year). The highest corrosion test rate (23 MPY) was reached in one week and was followed by a decrease to 8.8 MPY. Pitting evaluation by Shaw revealed that IN-9021-T452 exhibited significant pitting after 80 hours of immersion in 3.5% NaCl with "wormhole" type pits that were not related to the grain size.

In the present investigation, electrochemical techniques are used to characterize the corrosion behavior of the aluminum alloys IN-9052 and AA-6061-T6 exposed to NaCl environments. Because electrochemical techniques are straightforward and relatively fast, these techniques are quite valuable for studying corrosion, which is inherently a long-term process. Although the experimentally determined corrosion rates may not be representative of freely corroding specimens in actual applications, they are nonetheless useful as a method of comparison between materials exposed to the same conditions.

CHAPTER 3

EXPERIMENTAL

MATERIALS. IN-9052 and AA-6061-T6 samples were machined into 3/4" diameter flat discs from 1/8" sheet stock. Lead wires were attached to these samples and cold-mounted in an acrylic polymer. All samples where then wet-ground to a 600 SiC grit finish and degreased in acetone followed by a methanol rinse prior to exposure. Solutions were prepared from reagent grade chemicals and distilled water. Corrosion and galvanic-couple potentials are reported with respect to the saturated calomel electrode (SCE).

TEST METHODS. A Princeton Applied Research Model 351 Corrosion Test System was used to make all electrochemical measurements. A three electrode cell was used for polarization resistance (Rp), potentiodynamic polarization scans, and cyclic pitting scans. (See Figure 1.) Galvanic corrosion was studied by monitoring the current generated between the galvanic couples using the "351 system" as a zero-impedance ammeter. Galvanic coupling was accomplished by means of an electrical short-circuit with samples separated by a distance of 5 cm. (See Figure 1.)

Polarization Resistance. The polarization resistance (Rp) technique was used to measure a sample's uniform corrosion rate. Uniform corrosion rates were determined for freely corroding samples and for each sample immediately at the conclusion of galvanic testing. The Rp technique is useful because measurements can be made in short times without removing the sample from its environment, material destruction is minimal, corrosion rates can be monitored with time, and small corrosion rates can be measured. Briefly, Rp measurements involve the application of controlled-potential scan over a small range, typically ± 5 mV with respect to the corrosion potential, E_{corr}. In this potential range, the applied potential and current are linearly related to a close approximation. The resultant current is plotted against the applied potential and the slope of the straight line at the potential where the current passes through zero is equal to the polarization resistance. (See Figure 2.)

The theoretical relationship was first derived by Stern and Geary,[8] as shown below:

$$\Delta E / \Delta I = Rp = 1/I_{corr} \cdot B_a \cdot B_c / 2.303 (B_a + B_c) \quad (1)$$

or

$$I_{corr} = 1/Rp \cdot B_a \cdot B_c / 2.303 (B_a + B_c) \quad (2)$$

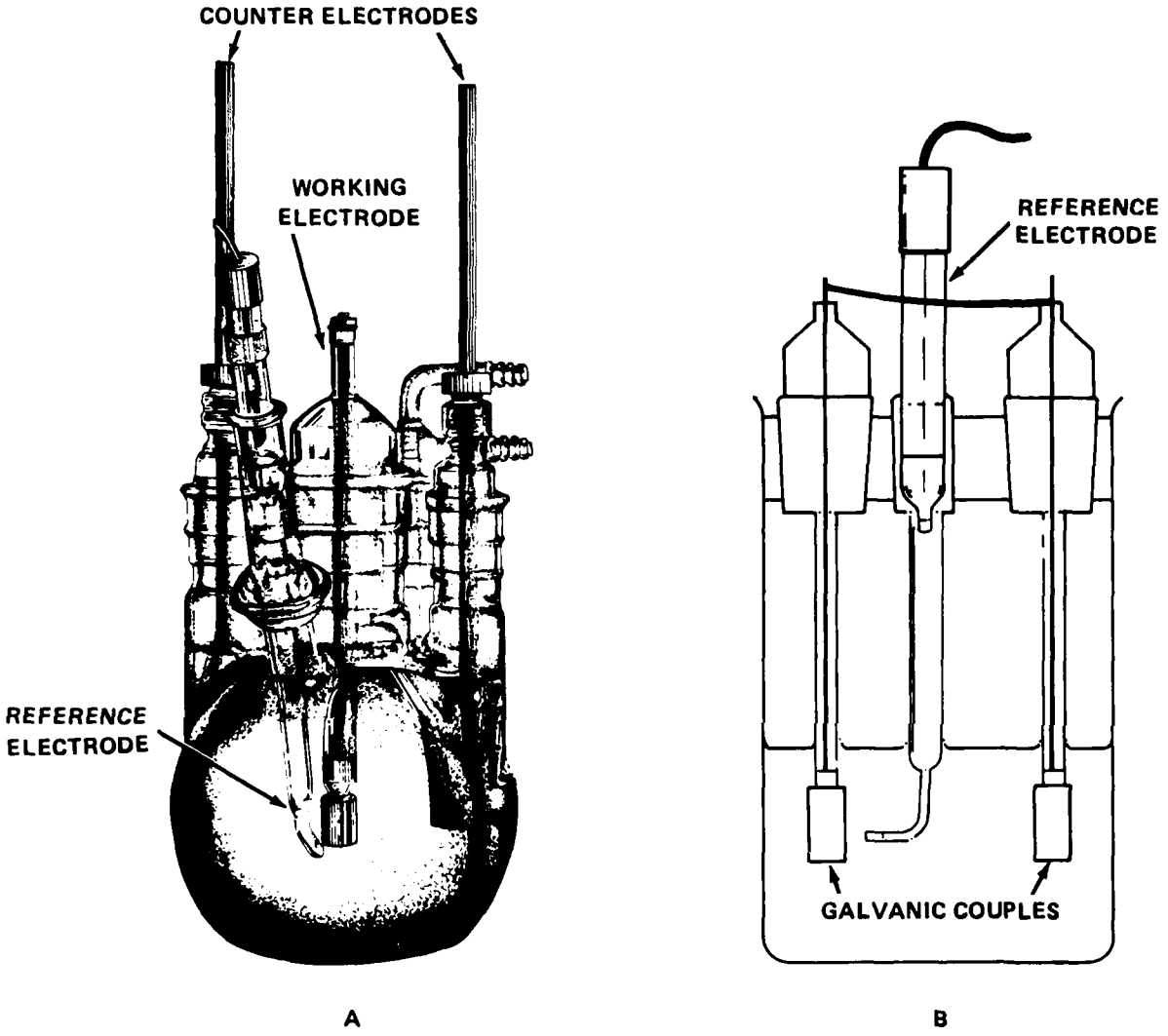

FIGURE 1. ELECTROCHEMICAL CORROSION TEST CELLS

A — CELL FOR ELECTROCHEMICAL MEASUREMENTS

B — GALVANIC CURRENT MEASUREMENT CELL

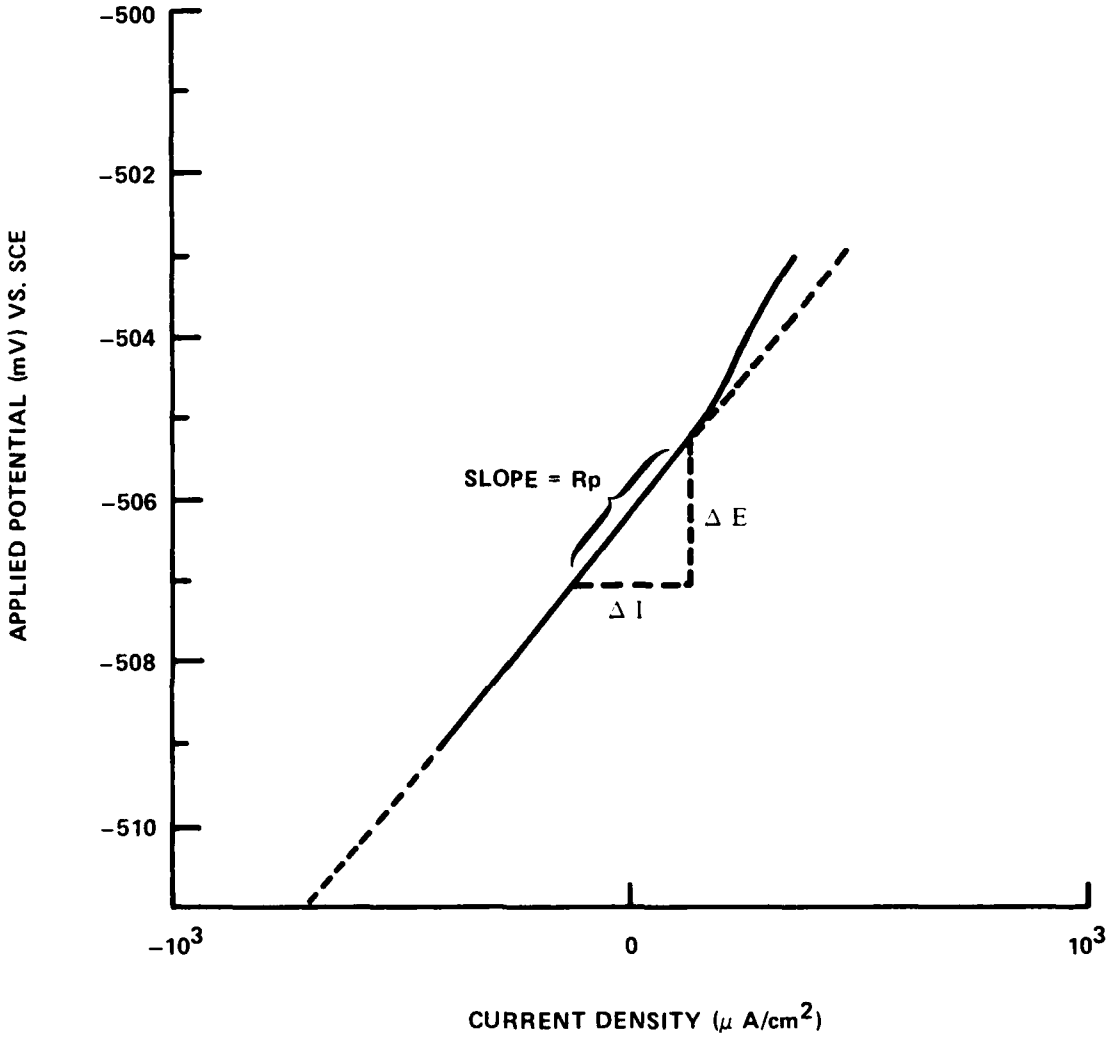

FIGURE 2. TYPICAL POLARIZATION RESISTANCE PLOT

where ΔE is the change in applied potential, ΔI is the corresponding change in current, B_a and B_c are the anodic and cathodic Tafel constants respectively, and I_{corr} is corrosion current. The calculated corrosion current can then be used to determine and represent the corrosion rate in more familiar terms, i.e., milli-grams per square decimeter per day (MDD), using the Faraday equation:

$$Q / F = W / EW \quad (3)$$

where Q is the number of coulombs (current x time), F is the Faraday constant (96,500 coulombs), W is the weight of the metal, and EW is the equivalent weight. Upon rearranging and substituting for the appropriate constants the following equation can be used to represent the corrosion rate as MDD:

$$MDD = 0.0895 \times I_{corr} \times EW / A \quad (4)$$

where A is the area of the exposed sample.

Equation (1) was derived for an "activation-controlled" process; however, for metals such as aluminum, the corrosion reaction is usually "diffusion-controlled". When corrosion reactions are "diffusion-controlled" equation (1) is simplified to,

$$Rp = 1/I_{corr} \times B_a/2.303 \quad (5)$$

Potentiodynamic Polarization. Cathodic and anodic polarization curves were obtained using a potentiodynamic technique. All samples were stabilized in 3.5% NaCl for 2 hours prior to measurement. The cathodic scan, at a rate of 0.3 mV/sec, was started at E_{corr} and scanned in the negative direction to a final value of -1.400 V (SCE). Anodic polarization curves were started at E_{corr} and scanned to more positive potentials, i.e. +400 mV vs. E_{corr}.

The potentiodynamic polarization technique was used to obtain experimental Tafel constant values for the anodic and cathodic reactions respectively. This technique can also be used to obtain corrosion current, I_{corr}, values by extrapolating back from the linear Tafel region to a point of intersection at E_{corr}, and to predict the initial galvanic current generated between two dissimilar metals by superimposing the anodic polarization curve of the more active material with the cathodic polarization curve of the more noble material. Typical polarization scans and examples of the electrode reactions can be seen in Figure 3.

Cyclic Pitting Scans. The pitting susceptibility of IN-9052 as compared to AA-6061-T6 was determined using a potentiodynamic cyclic polarization technique. The cyclic scan was started at

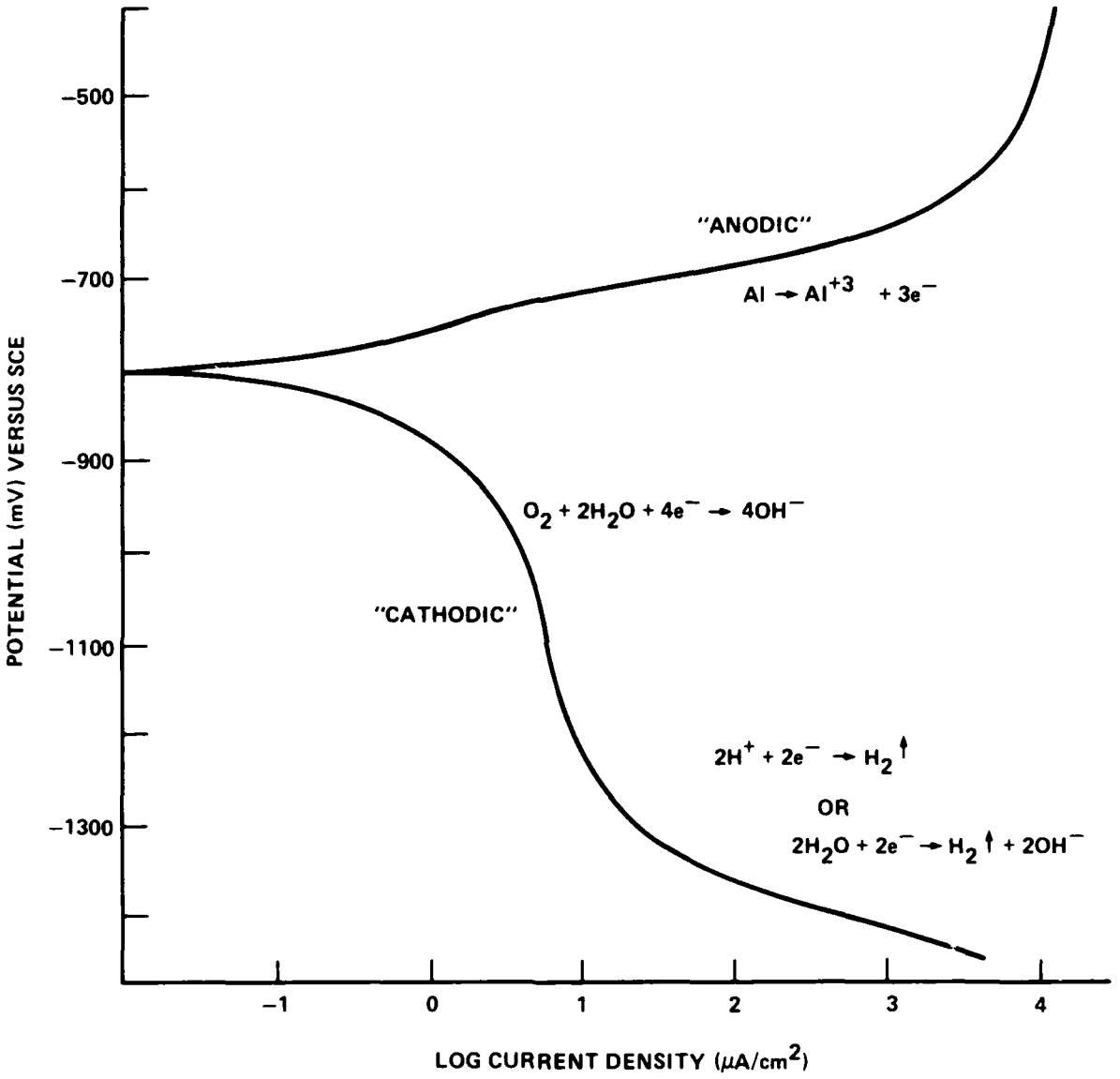

FIGURE 3. EXAMPLES OF POTENTIODYNAMIC POLARIZATION CURVES, INCLUDING TYPICAL ANODIC AND CATHODIC ELECTRODE REACTIONS

E_{corr} and the potential increased in the positive (anodic) direction. The corresponding current will at some potential increase rapidly, indicating localized breakdown of the oxide film, i.e. pitting. The potential at which the current increases rapidly is known as the characteristic pitting potential, E_p, of the metal. At a preselected current, the scan is reversed, and during scan reversal pit formation ceases and existing pits repassivate. For example, the presence of a hysteresis loop in the cyclic polarization scan indicates that the metal is susceptible to pitting. (See Figure 4.) On the other hand, a reverse scan that traces the forward scan indicates that test metal is resistant to pitting. (See Figure 5.) This technique is useful for screening the resistance of an alloy to passive film breakdown.

For this study, samples were immersed in de-aerated 0.1M NaCl and allowed to stabilize for two hours prior to testing. The 0.1M NaCl solution was de-aerated with nitrogen for about 18 hours prior to introduction of the test sample. Pitting scans were started at E_{corr} and scanned in the positive direction at a rate of 0.2 mV/sec, and reversed at 75-100 μA.

Galvanic Current Measurements. Unlike other electrochemical techniques, galvanic corrosion experiments do not involve the application of an applied potential. When two dissimilar metals are placed in the same environment a potential difference develops, and when electrical contact is made between the metals a current flows. The magnitude of this "galvanic" current determines the severity of corrosion.

Galvanic corrosion was studied by monitoring the current generated between dissimilar metals using a zero-impedance ammeter, incorporated into the model 351 system. Galvanic currents were measured for one hour every day (excluding weekends) for times up to 900 hours. Galvanic data is presented as a plot of galvanic current density against time.

Pit Morphologies. Scanning electron microscopy (SEM) was used to study the morphologies of pit development for freely corroding samples exposed to 3.5% NaCl. Samples of IN-9052 and AA-6061 were wet ground to a 600 Sic grit finish, and then coated with Amercoat 90* along the edges and the backside, exposing only one surface. The samples were suspended in a 3.5% NaCl solution, under ambient conditions, for five weeks. Distilled water was periodically

* A trademark of AM Chem Products.

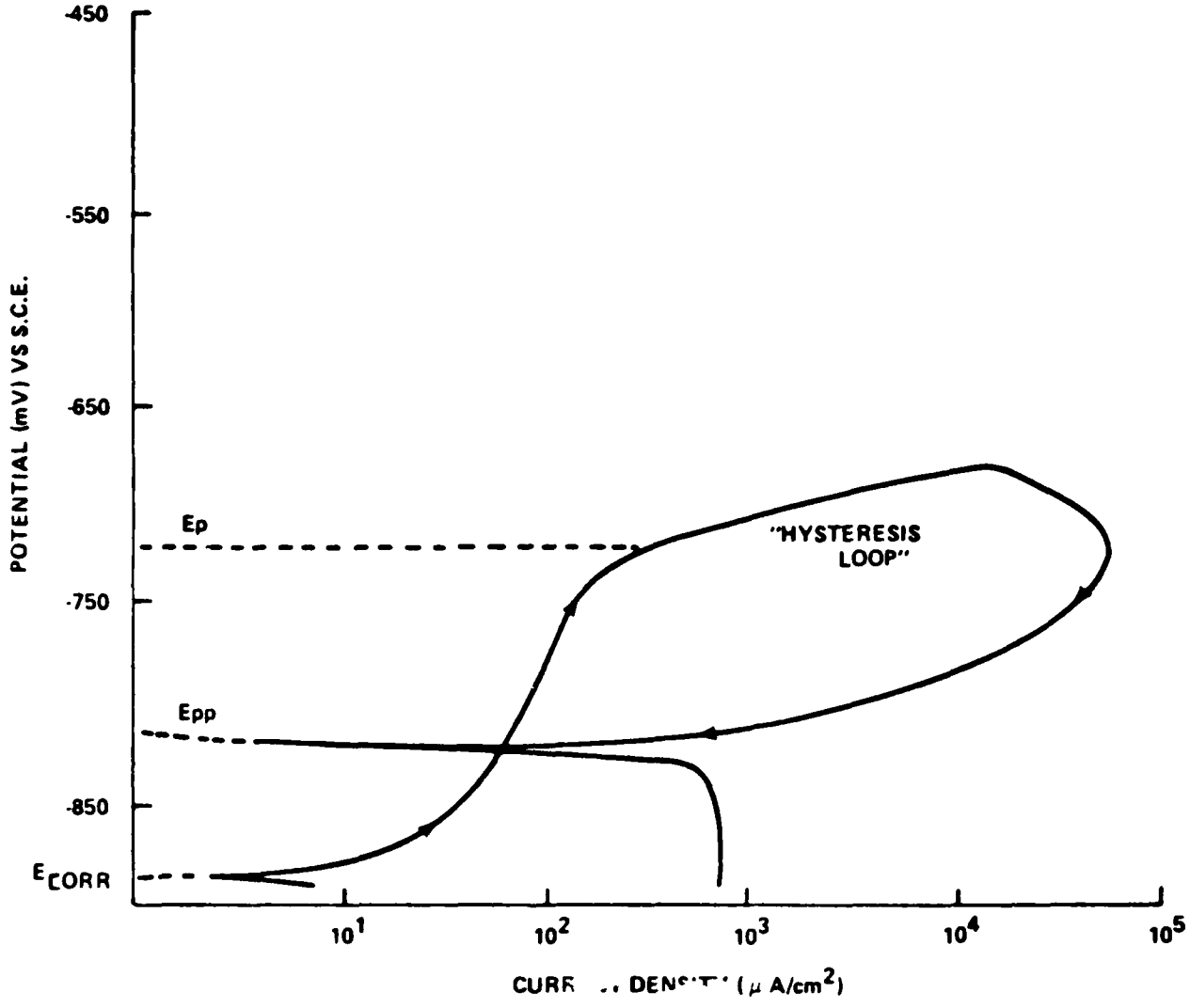

FIGURE 4. POTENTIODYNAMIC PITT SCAN FOR AN ALUMINUM COMPOSITE I[illegible] % NaCl

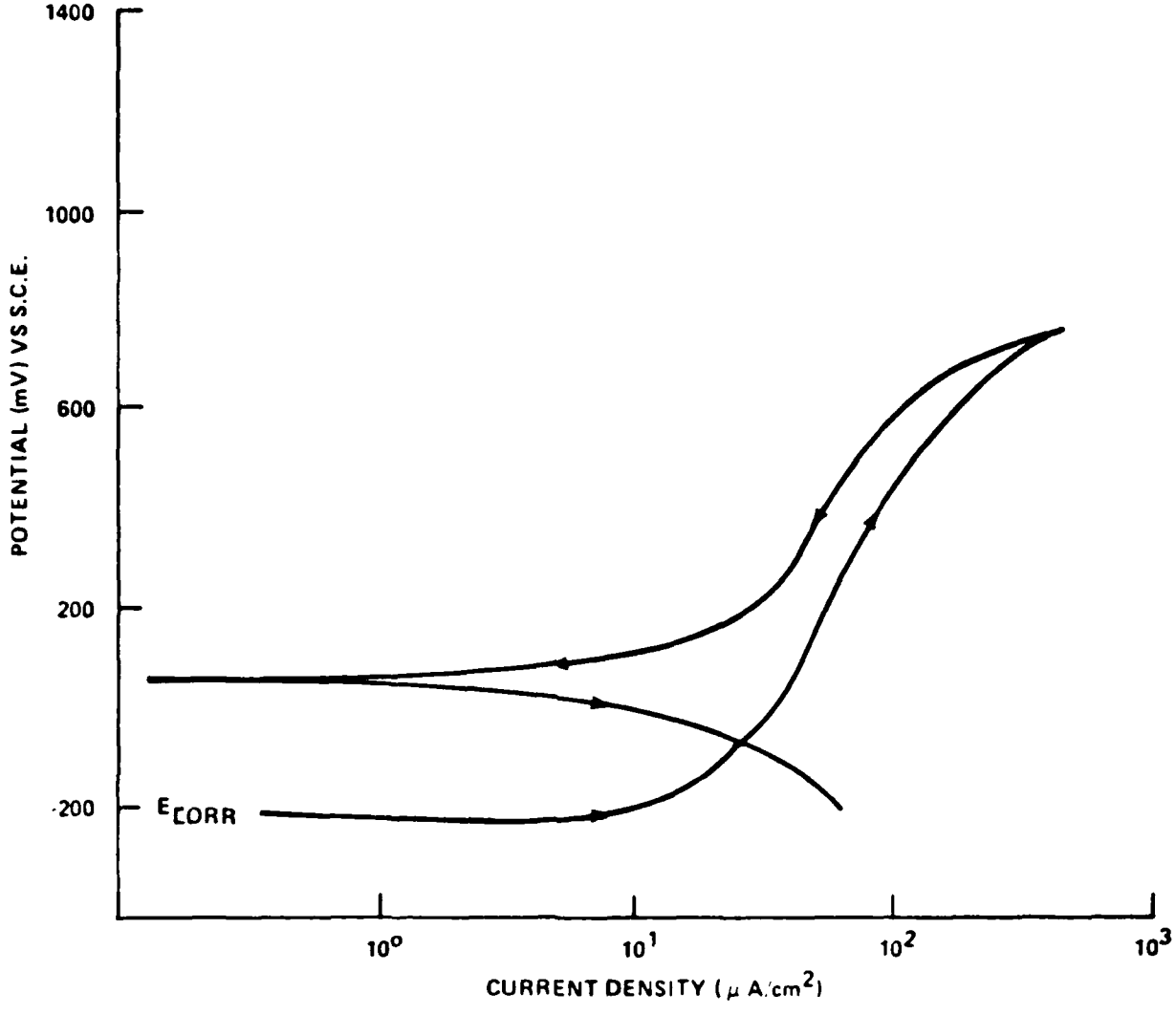

FIGURE 5. POTENTIODYNAMIC PITTING SCAN FOR AA-2024 IN 1.0N $NaNO_3$

added to the test vessel to replace water loss due to evaporation. After removal from solution, the samples were rinsed with distilled water and dried in an air stream. The samples were then examined using SEM. After initial examination, corrosion films which formed during exposure were removed with 30% NaOH (a cotton swab applicator was used to apply the NaOH which was followed by immediate rinsing with liberal amounts of distilled water to reduce attack of the underlying metal) and re-examined with the SEM.

CHAPTER 4

RESULTS AND DISCUSSIONS

UNIFORM CORROSION. Rp measurements were used to compare the uniform corrosion rates of IN-9052 and AA-6061-T6. Although it's difficult to calculate exact corrosion rates using this technique, the magnitude of Rp values can be used to compare different materials exposed to the same environment; therefore, a qualitative comparison is possible. In addition, it must be emphasized that the Rp technique gives instantaneous corrosion rates and the value of the technique lies in its ability to predict trends in the corrosion rate with time. For example, it is of interest to determine whether the corrosion rate increases with time, remains constant, or decreases with time. Therefore, Rp results will be used, in general, to discuss trends in the corrosion rate.

The uniform corrosion of IN-9052 and AA-6061 exhibited different behavior. (See Figures 6-7.) The corrosion rate for IN-9052 increased with time at early stages of corrosion and then decreased to a final "steady-state" corrosion rate.* (See Figure 6.) On the other hand, the corrosion rate of AA-6061 decreased initially; however, at later times the corrosion rate accelerated, and eventually reached a "steady-state" value. (See Figure 7.) The steady-state corrosion rate for IN-9052 was lower than the steady-state rate for AA-6061 as shown by Rp values of 14,000 ohms.cm^2 and 15,000 ohms.cm^2 respectively.

Both IN-9052 and AA-6061 exhibited pitting attack. However, pitting on AA-6061 appeared to be more severe and more frequent than observed for IN-9052. The surface of AA-6061 was significantly discolored (i.e., dark gray) and some corrosion product build-up was detected. IN-9052 remained bright in appearance and only a minimal amount of corrosion products could be seen.

POTENTIODYNAMIC POLARIZATION. The anodic polarization curves for IN-9052 and AA-6061 were nearly identical. The shapes of the curves were similar and the anodic currents were of the same order of magnitude. (See Figures 8-9.) Measured anodic Tafel constants of 34 and 27 mV/decade were obtained for IN-9052 and AA-6061 respectively. The fact that the anodic Tafel constants were nearly identical suggested that the mechanisms for anodic dissolution were the same.** However, inspection of these samples under an optical

*Remember that the Rp value is inversely proportional to the corrosion current, i.e., a large Rp value is equivalent to a low corrosion rate.

**The value of a Tafel constant is dependent on the mechanism responsible for reaction at an electrode.

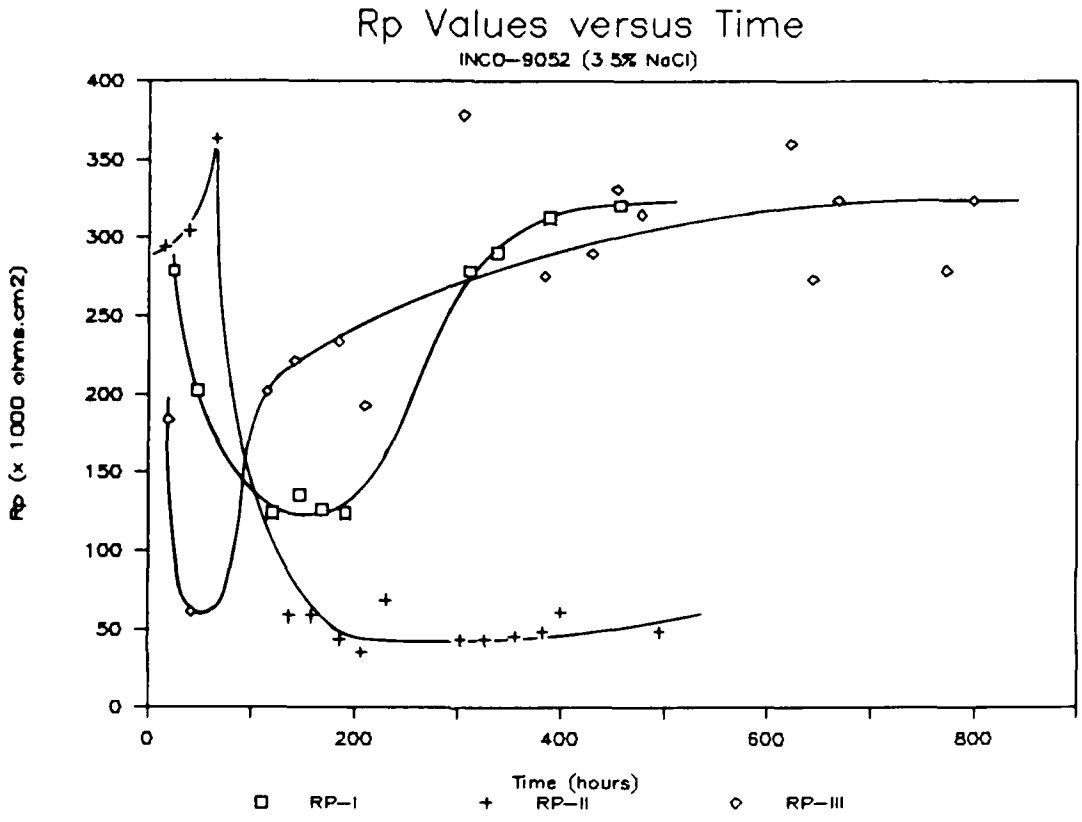

FIGURE 6. Rp - TIME PLOTS FOR IN-9052 EXPOSED TO 3.5% NaCl

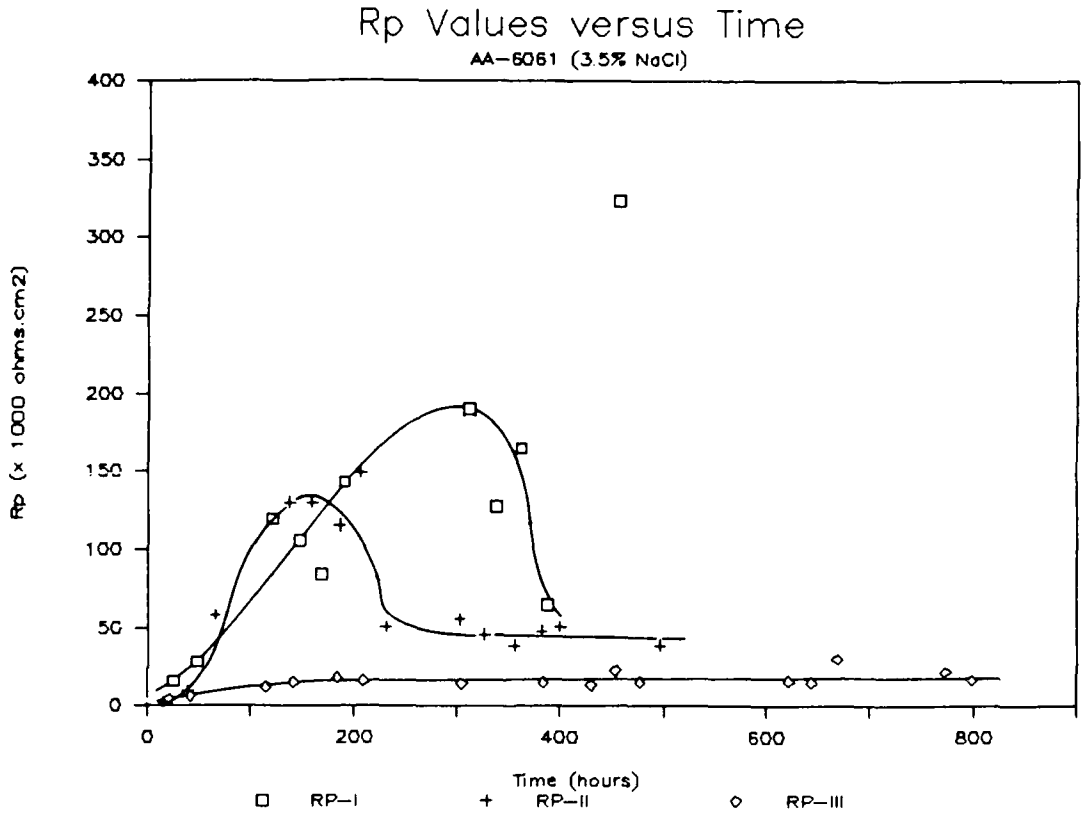

FIGURE 7. Rp - TIME PLOTS FOR AA-6061 EXPOSED TO 3.5% NaCl

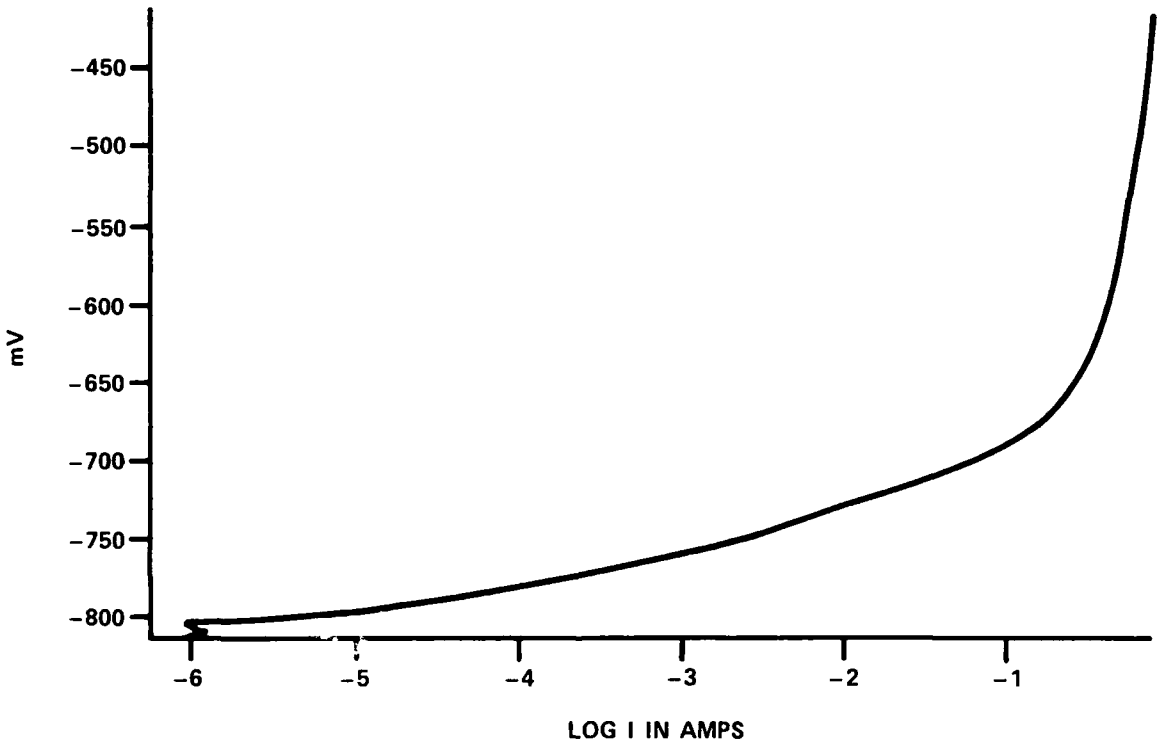

FIGURE 8. POTENTIODYNAMIC ANODIC POLARIZATION CURVE FOR IN-9052 EXPOSED TO 3.5% NaCl

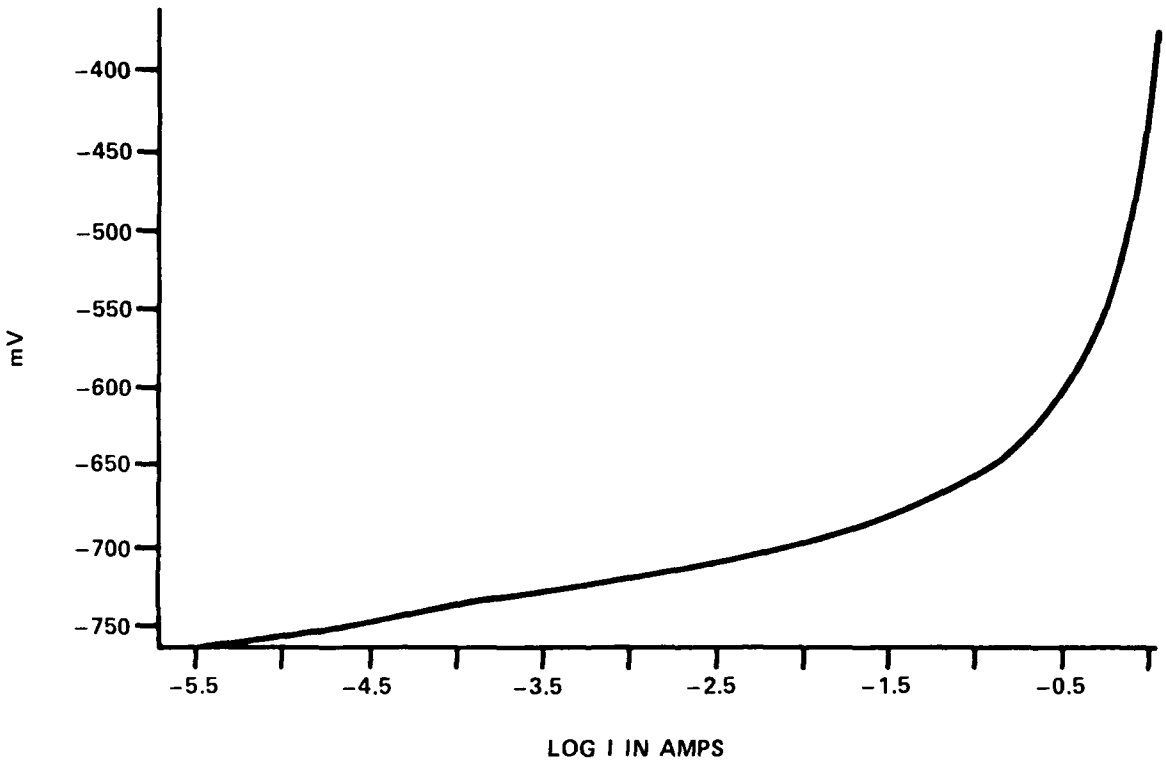

FIGURE 9. POTENTIODYNAMIC ANODIC POLARIZATION CURVE FOR AA-6061 EXPOSED TO 3.5% NaCl

light microscope (17X) revealed that the nature of attack was different for each sample. AA-6061 was so severely pitted that the pits gave the appearance of a surface uniformly attacked. Conversely, IN-9052 revealed a large number of small pits in the center of the specimen, and a preference for edge corrosion or crevice corrosion, as evidenced by the increased corrosion in the region between the metal and the polymeric material encasing the sample. Although the Tafel constants indicated that similar anodic dissolution mechanisms were operative, the nature of corrosion was different for the two alloys.

Cathodic polarization behavior was similar for both IN-9052 and AA-6061. The shapes of the cathodic curves indicated that the cathodic reduction reaction was "diffusion-controlled".* This behavior is typical of alloys exposed to neutral aqueous NaCl environments. For this behavior, the cathodic current is often called the limiting diffusion current, I^c_{L,O_2}. The values of the $I_{L,O}$ for IN-9052 and AA-6061 were 1.13 and 4.6 $\mu A/cm^2$ respectively. This indicated that the reduction of oxygen was sluggish and, therefore, controlled the rate of corrosion.

CALCULATED CORROSION RATES. Corrosion rates were calculated using equations (5) and (4) for both IN-9052 and AA-6061. Because of the uncertainty in the change of anodic Tafel constants with time, a range of Tafel constants was used in equation (5) to calculate a range of corrosion rates. The Tafel ranges for both samples were selected so the experimentally measured anodic Tafel constant fell in the middle, e.g., the measured Tafel constant for IN-9052 was 34 mV/decade, thus, a range of 20-52 mV/decade was used. The corrosion rate for IN-9052 was nearly the same at early times and at times where the Rp value reached a "steady-state"; results revealed that the corrosion rate for IN-9052 should fall between about .03 and .078 MDD. (See Figure 10.) This range of corrosion rates was somewhat lower than the corrosion rate reported by Erich and Donachie (6) for IN-9052-F of 0.1 MDD (exposed to alternate immersion in 3.5% NaCl). For AA-6061, the measured anodic Tafel constant was 27 mV/decade and the range of Tafel constants tested was to 44 mV/decade. The corrosion rates at earlier times were an order of magnitude higher than those at "steady-state"; where the corrosion rate for AA-6061 at early times fell between 2.0 and 7.0 MDD and between .10 and .25 MDD at "steady-state". (See Figure 11.) These results indicated that the uniform corrosion rate of IN-9052 was lower by an order of magnitude in comparison to AA-6061.

*"Diffusion-control" occurs when the rate of a reaction, in this case, the cathodic reduction of oxygen, is limited by the rate at which the reducing species migrates to the electrode surface.

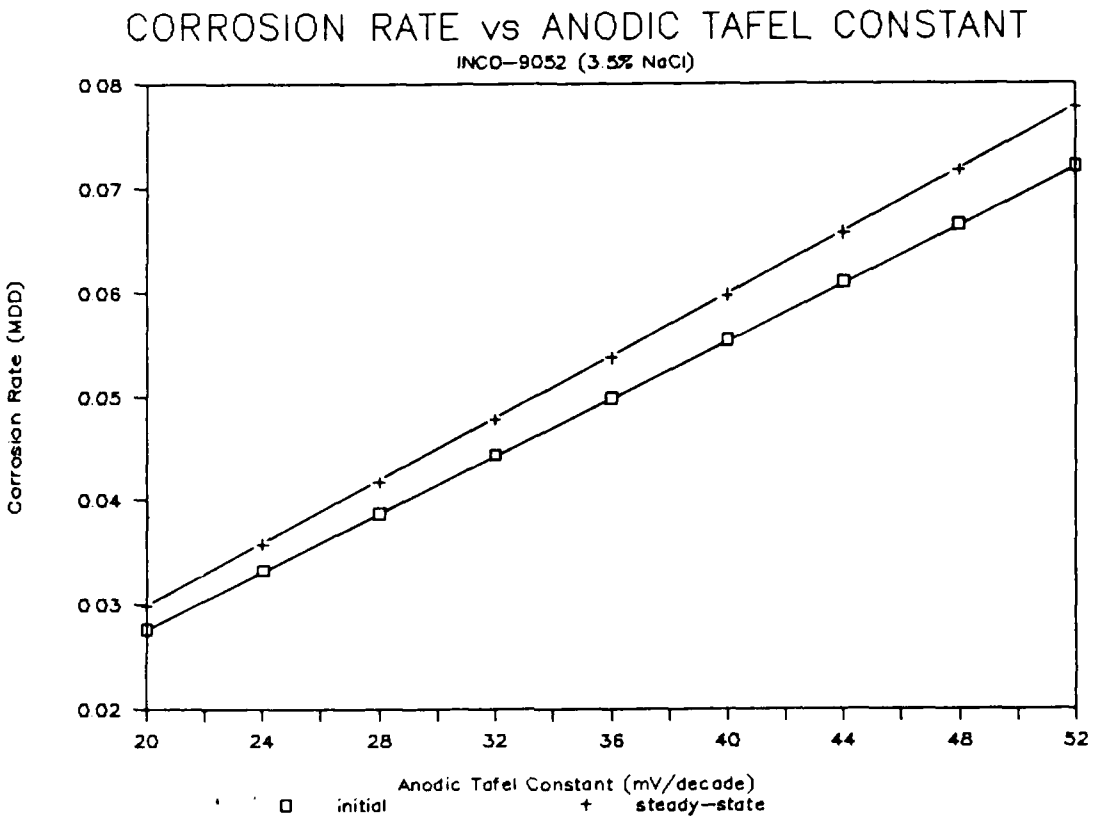

FIGURE 10. CORROSION RATE - ANODIC TAFEL CONSTANT PLOT FOR IN-9052 EXPOSED TO 3.5% NaCl

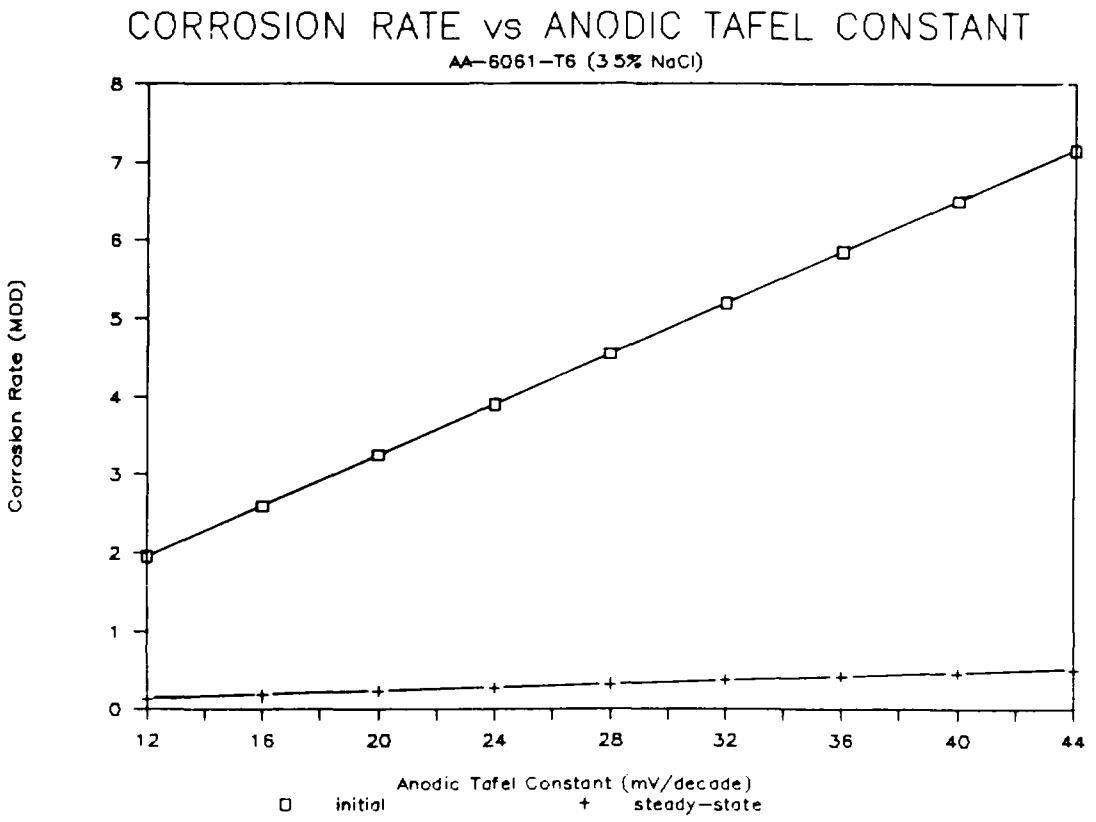

FIGURE 11. CORROSION RATE - ANODIC TAFEL CONSTANT PLOT FOR AA-6061 EXPOSED TO 3.5% NaCl

CYCLIC PITTING SCANS. Because of the inherent protective nature of aluminum alloy oxides, corrosion in neutral NaCl environments involves localized attack, i.e., pitting. Cyclic pitting scans are designed to ascertain a metal's susceptibility to pitting, where the shape of the cyclic potentiodynamic curve indicates whether pitting is to be expected. In addition, the characteristic pitting potential, E_p, is used to make comparisons between different metals. For example, the more positive the value of E_p the more resistant the metal is to pitting and the greater the separation of E_p from E_{corr} the more resistant the metal is to pitting. Both IN-9052 and AA-6061 exhibited a hysteresis loop which was indicative of pitting. (See Figures 12-13.) The E_p for AA-6061 was -702 mV, which was about 98 mV more positive than its "steady-state" E_{corr} value (ca., -800 mV). For IN-9052, E_p was slightly more negative, -749 mV; however, in this case, E_p was about 400 mV more positive than "steady-state" E_{corr} (ca., -1.150 mV). These results showed that both IN-9052 and AA-6061 were susceptible to pitting corrosion in 3.5% NaCl; however, based on the difference between E_p and E_{corr}, IN-9052 should be somewhat more resistant to pitting. Although IN-9052 will ultimately pit, it may be that pit initiation times were greater for IN-9052. This, however, must be confirmed with other electrochemical techniques specifically designed to determine pit initiation times.

GALVANIC CORROSION. The physical or electrical connection of two dissimilar metals can result in accelerated corrosion for one metal of the couple (anode), while the other metal is protected (cathode). Because of the need to utilize a variety of different metals to construct complex structures as dictated by increasing mechanical, metallurgical, and economical requirements, it is important to determine in advance the severity of potential galvanic interaction. Several types of dissimilar metals are currently used in the warhead hull of the MK-50 torpedo; therefore, the galvanic behavior of IN-9052 and AA-6061 coupled to SS-316 and IN-9052 coupled to AA-6061 were investigated.

A measurement of galvanic current with time is valuable to determine the magnitude of corrosion and the behavior of the galvanic corrosion rate. The direction of current flow can usually be determined by the individual E_{corr} values in that environment. The metal with the most positive E_{corr} value will behave as the cathode and the metal with the more negative value the anode. It is the more negative metal which usually experiences accelerated corrosion. The magnitude of the current generated is dependent on several variables, including: the cathode-to-anode surface area ratio, kinetics of the cathodic reaction at the cathode, initial presence or subsequent formation of corrosion product films, solution agitation, and temperature.

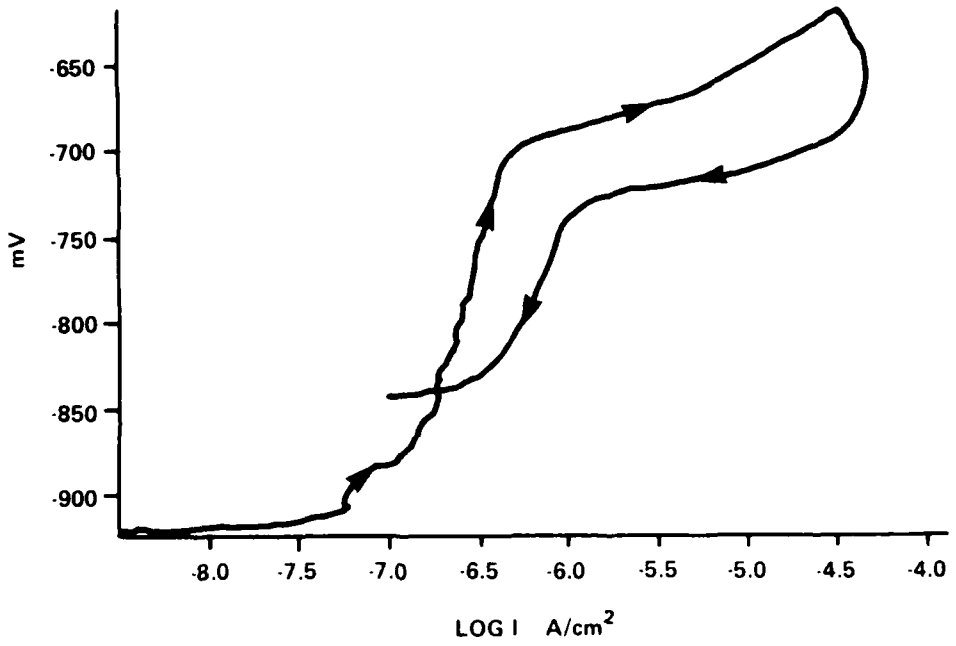

FIGURE 12. CYCLIC PITTING SCAN FOR AA-6061 EXPOSED TO DE-AERATED 0.1M NaC1

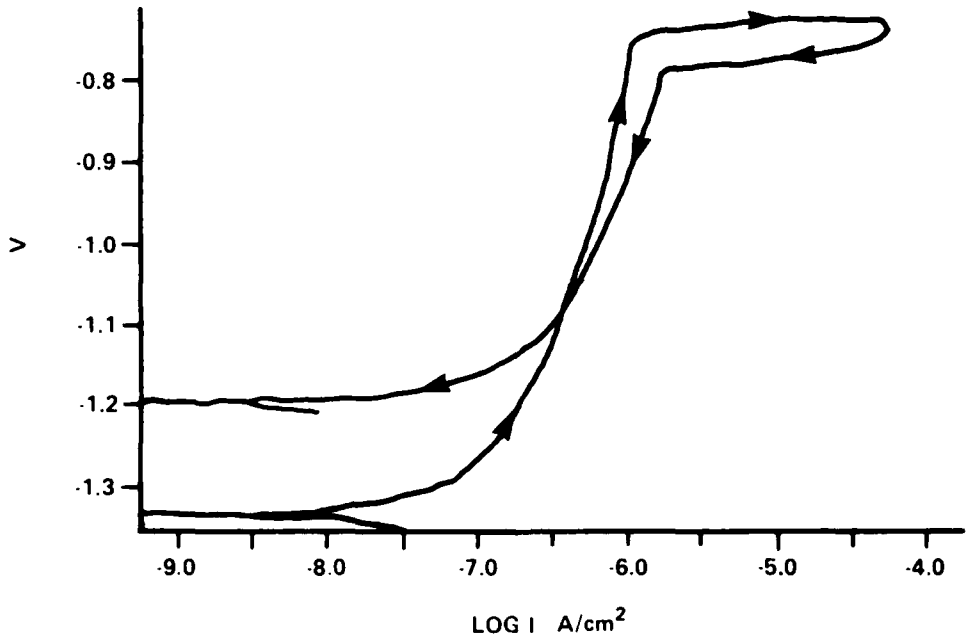

FIGURE 13. CYCLIC PITTING SCAN FOR IN-9052 EXPOSED TO DE-AERATED 0.1M NaC1

For this investigation, the cathode-to-anode area ratio was considered to be the most important controlling factor. A large cathode-to-anode area ratio can result in the production of large galvanic currents, i.e., high corrosion rates. Experimental measurements revealed that SS-316 had a more positive E_{corr} value than IN-9052 or AA-6061 and, thus, as expected, behaved as the cathode. Because the cathode-to-anode area ratios for the SS-316/IN-9052 and SS-316/AA-6061 galvanic couples in the MK 50 system are small, small galvanic currents were expected. (For this study, a cathode-to-anode area ratio of 0.111 was used.) This behavior was observed at early times for the SS-316/IN-9052 couple; however, after 200 hours the galvanic current began to increase, eventually reaching a steady value of about 13 $\mu A/cm^2$. (See Figure 14.) After inspection of the IN-9052 sample it was discovered that extensive corrosion had occurred beneath the organic coating at the specimen's edge. This observation indicated that a crevice corrosion site developed in this region which led to accelerated corrosion and the consequential increase in galvanic current. Corrosion at early times involved general and/or pitting at the center of the specimen. Because galvanic corrosion for this couple was "cathodic-controlled" mixed potential theory predicts that the following equation can be used to calculate the dissolution current density at the IN-9052 anode:[9-11]

$$i_d^a = i_{gal} + i_{L,O_2}^a \qquad (6)$$

where i_d is the dissolution current density at the anode, i_{gal} is the measured galvanic current density, and i_{L,O_2}^a is the limiting diffusion current density for oxygen reduction at the anode. Corrosion rates can then be calculated using equations (3) and (4). In addition, Rp values obtained at the conclusion of galvanic testing were used to calculate an instantaneous corrosion rate for the IN-9052 anode. A summary of predicted corrosion using equation (6) and measured instantaneous corrosion rates are given in Table 2. Corrosion rates were calculated at early and final times of testing. Also, in Table 2, corrosion rates calculated for uncoupled samples obtained from Rp measurements are supplied to compare with rates predicted by galvanic current density results. For this galvanic couple, the initial corrosion rate for IN-9052 was two orders of magnitude higher than observed for uncoupled IN-9052. The corrosion rate increased by three orders of magnitude at 692 hours. Rp measurements made immediately after galvanic testing gave a corrosion rate of 2.1 MDD, less than predicted using equation (6) but still two orders of magnitude higher than observed for uncoupled IN-9052.

A second SS-316/IN-9052 couple was studied using a different organic coating to protect the specimen from edge corrosion. The

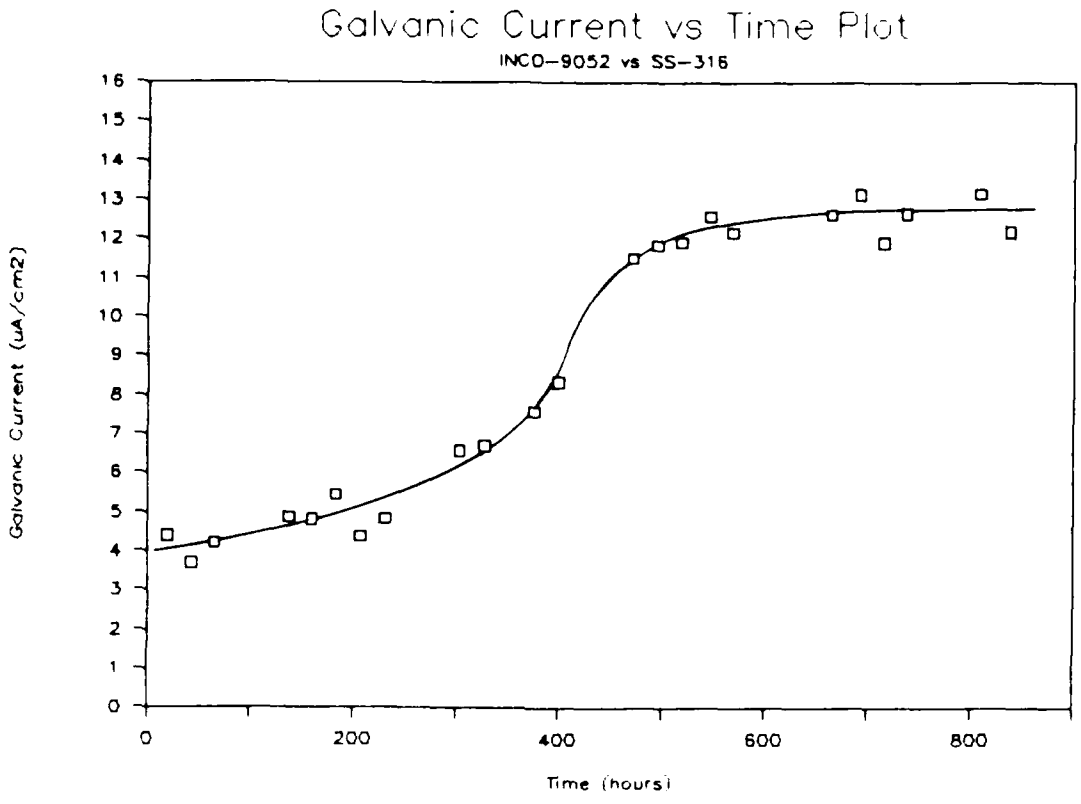

FIGURE 14. GALVANIC CURRENT DENSITY - TIME PLOT FOR A IN-9052/SS-316 COUPLE EXPOSED TO 3.5% NaCl

TABLE 2. SUMMARY OF PREDICTED CORROSION RATES USING MIXED-POTENTIAL THEORY AND CORROSION RATES CALCULATED FROM Rp MEASUREMENTS

Couple Cathode/Anode	r_d (mdd) Start	r_d (mdd) End	r_u (mdd) Start	r_u (mdd) End	r_g (mdd) End
SS-316/IN-9052	5.28	16.54	.046	.050	2.1
SS-316/IN-9052	9.09	7.85	.046	.050	2.5
SS-316/AA-6061	8.08	7.47	4.20	.15	1.4

r_d - predicted corrosion rate of anode using galvanic current measurments and the "mixed-potential" theory

r_u - corrosion rate of uncoupled anode

r_g - corrosion rate of anode measured after uncoupling from SS-316

magnitude of the galvanic current for this sample was lower than observed for the first SS-316/IN-9052 couple, indicating that crevice corrosion contributions were absent or reduced using the new protective coating. The predicted corrosion rates at 1317 hours using equation (6) was 7.85 MDD, which was lower than that observed for the first SS-316/IN-9052 couple tested. A corrosion rate of 7.9 MDD was obtained at 800 hours using equation (6) which was two orders of magnitude higher than observed for uncoupled IN-9052 at 800 hours. Rp results gave a corrosion rate for coupled IN-9052 of 2.5 MDD, similar to the first sample, which was lower than the predicted value but still two orders of magnitude higher than observed for uncoupled IN-9052.

In comparison, the galvanic current for SS-316/AA-6061 was small and remained constant for the duration of the test period. (See Figure 15.) AA-6061 exhibited only localized pitting with the build-up of some corrosion products. In fact, the galvanic corrosion rates at initial times and final times were nearly the same. (See Table 2.) Predicted corrosion rates were slightly lower than observed for coupled IN-9052 but values were also two orders of magnitude higher than observed for uncoupled AA-6061. This indicated that galvanic corrosion may be slightly greater for IN-9052 when coupled to SS-316 but both galvanic couples gave corrosion rates that were at least two orders of magnitude higher than observed for uncoupled IN-9052 or AA-6061. It might be argued that crevice interaction for the IN-9052/SS-316 couple contributed to the observed higher corrosion rates for IN-9052 compared to those predicted for AA-6061.

Because a small SS-316 surface area was used, the generated galvanic currents were small. For example, if equivalent surface areas had been studied, the initial galvanic current densities would have been about 25.1 and 28.2 $\mu A/cm^2$ for SS-316/IN-9052 and SS-316/AA-6061 respectively. The initial galvanic currents were obtained from the overlay of the cathodic polarization curve for SS-316 and the anodic polarization curves for AA-6061 and IN-9052, the intersection of these curves was taken to be equivalent to the initial galvanic current densities. (See Figures 16-17.)

A galvanic couple between IN-9052 and AA-6061 with equivalent surface areas was tested. Based on E_{corr} values for uncoupled IN-9052 and AA-6061, AA-6061 should behave as the cathode and IN-9052 the anode, i.e., E_{corr} for AA-6061 was more positive than E_{corr} for IN-9052. (See Figure 18.) Galvanic current measurements indicated that IN-9052 was the anode; however, the magnitude of the galvanic current density was small (ca., 1.4 $\mu A/cm^2$). (See Figure 19.) Typically, when aluminum alloys behave as the cathode in a

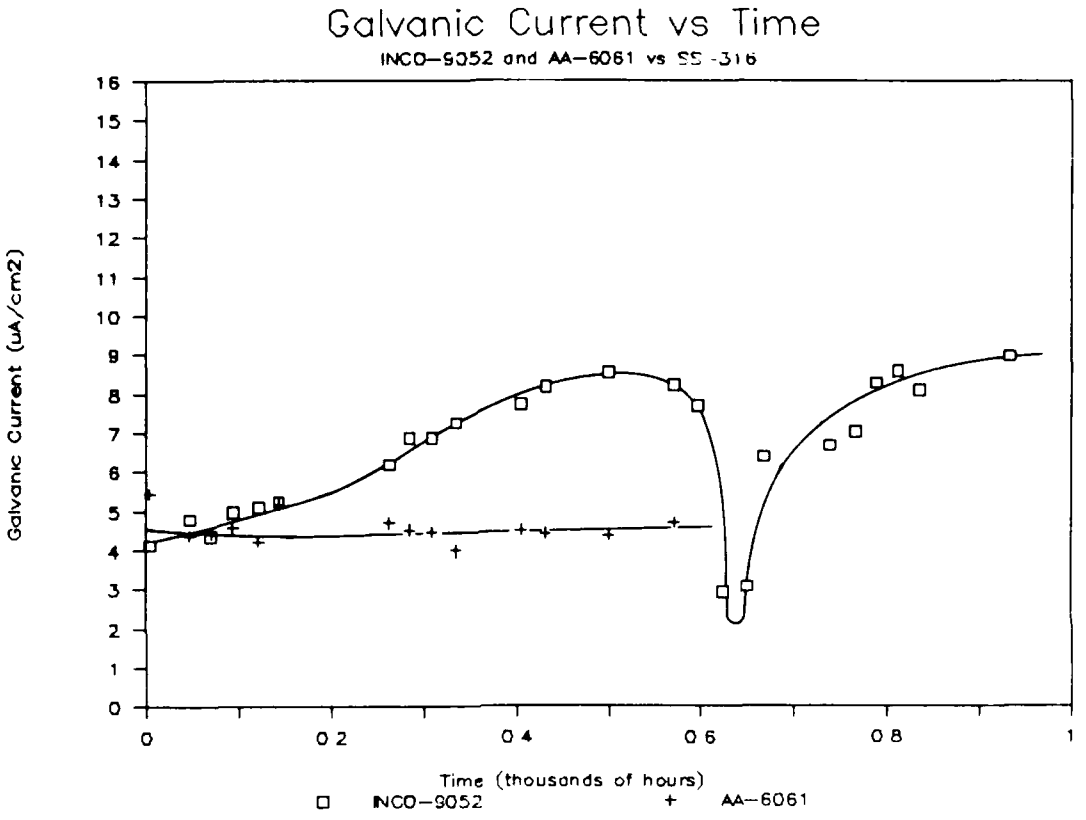

FIGURE 15. GALVANIC CURRENT DENSITY - TIME PLOT FOR IN-9052/SS-316 AND AA-6061/SS-316 COUPLES EXPOSED TO 3.5% NaCl

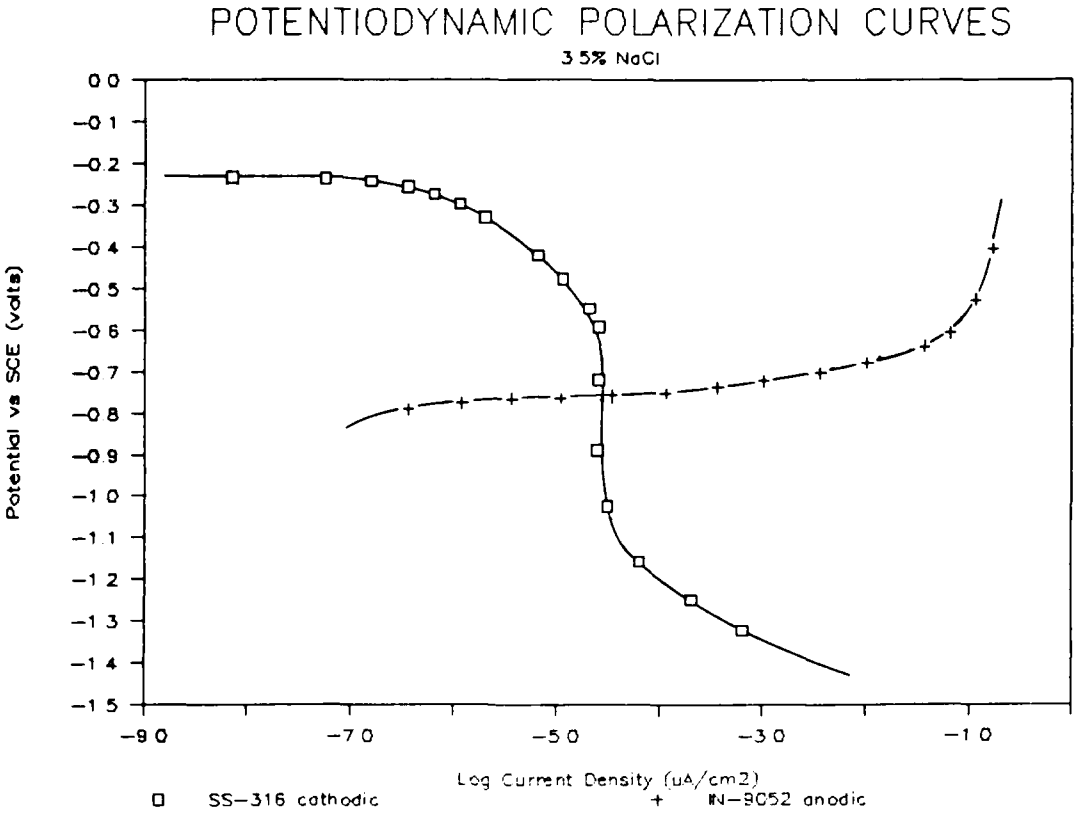

FIGURE 16. OVERLAY OF ANODIC POLARIZATION CURVE OF IN-9052 AND CATHODIC POLARIZATION CURVE OF SS-316, EXPOSURE TO 3.5% NaCl

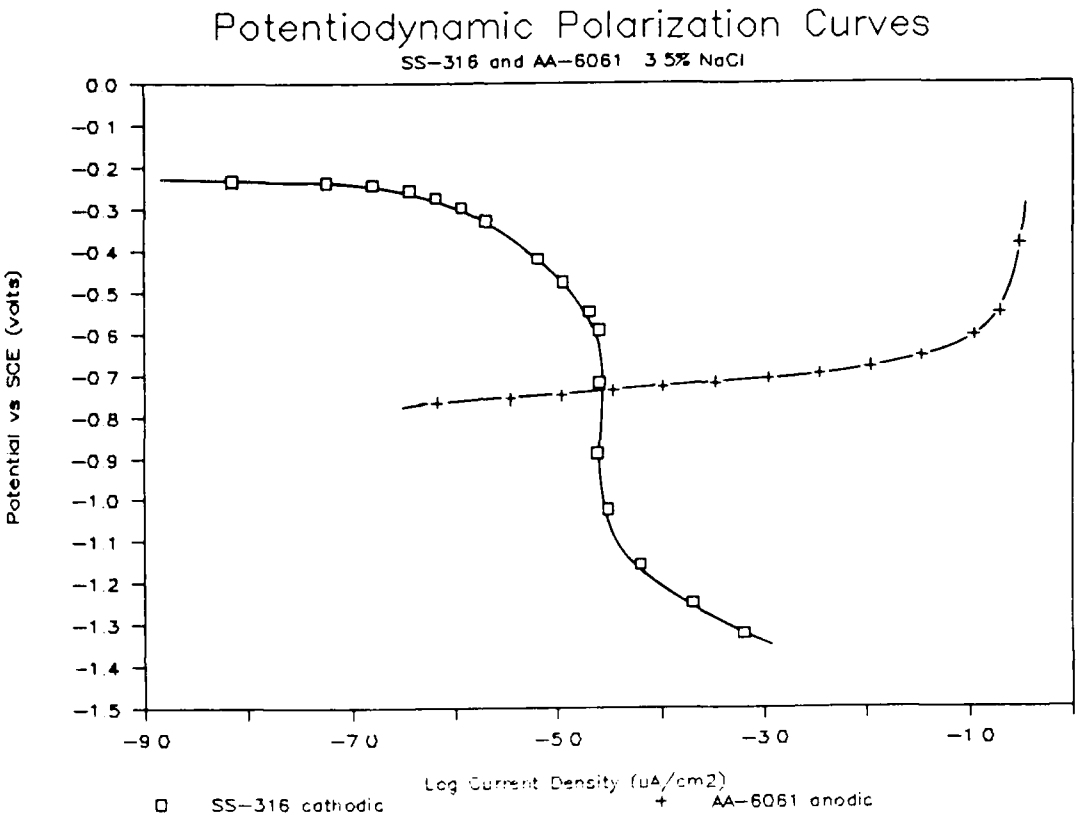

FIGURE 17. OVERLAY OF ANODIC POLARIZATION CURVE OF AA-6061 AND CATHODIC POLARIZATION CURVE OF SS-316, EXPOSURE TO 3.5% NaCl

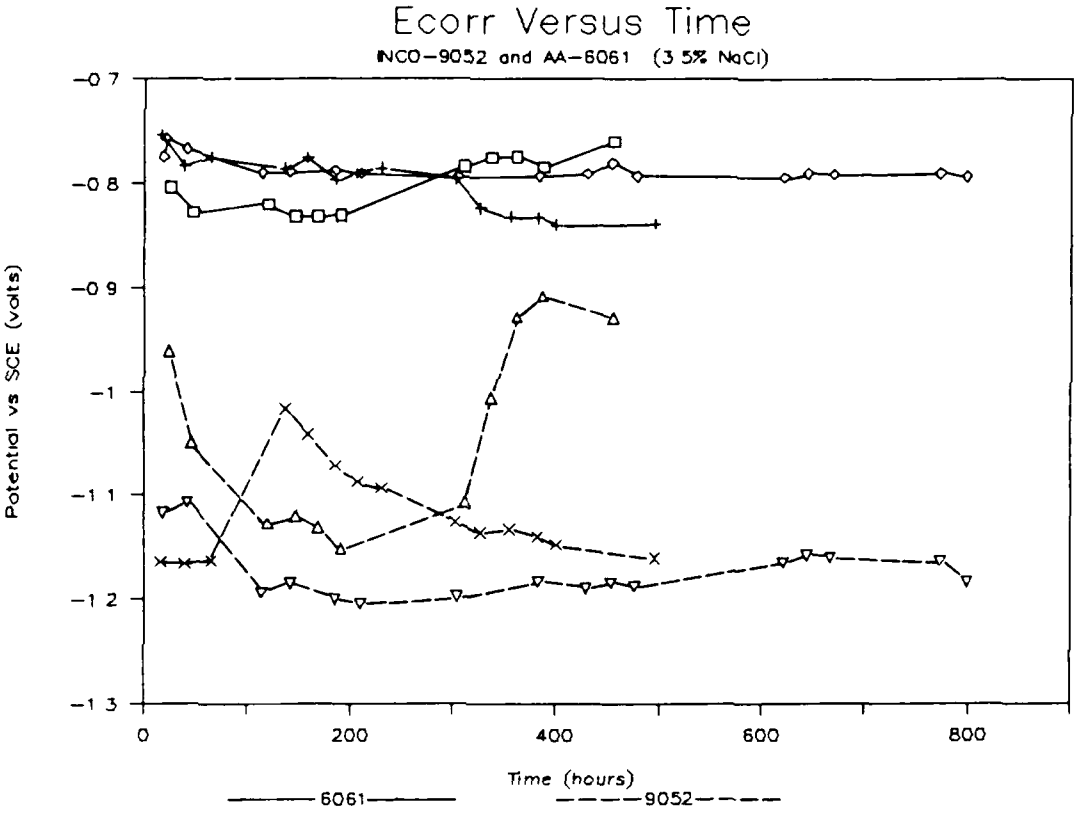

FIGURE 18. Ecorr - TIME PLOTS FOR IN-9052 AND AA-6061, EXPOSURE TO 3.5% NaCl

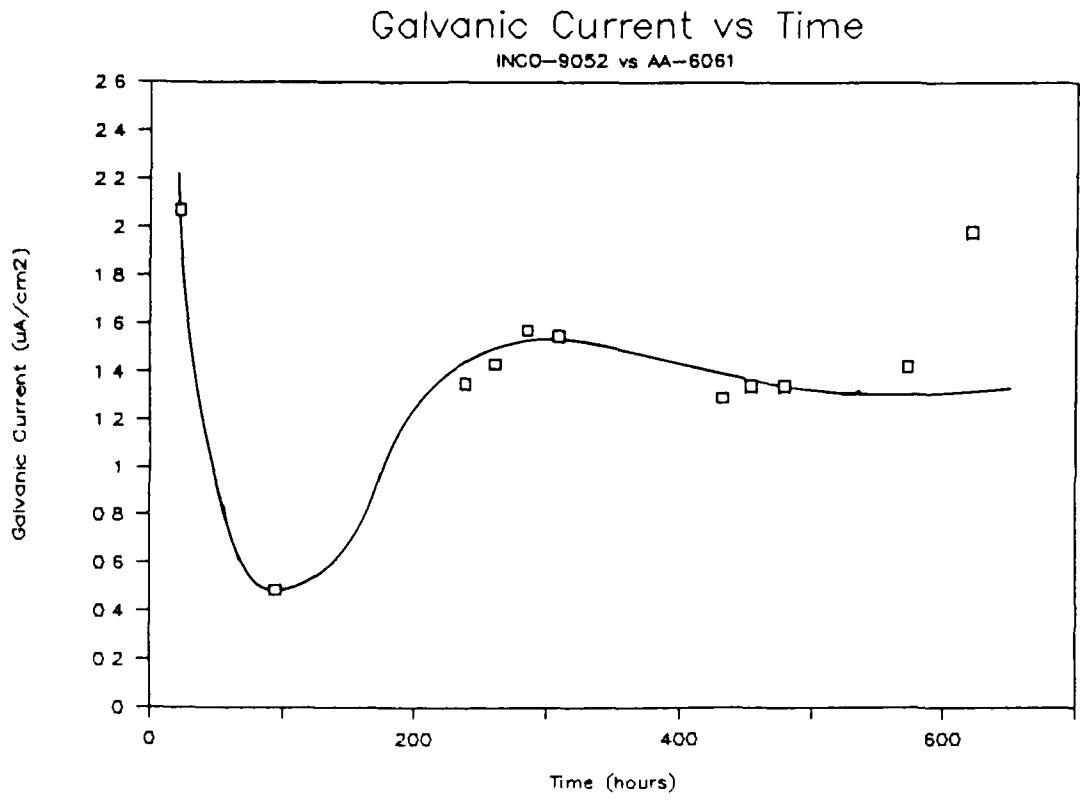

FIGURE 19. GALVANIC CURRENT DENSITY - TIME PLOT FOR A IN-9052/AA-6061 COUPLE EXPOSED TO 3.5% NaCl

galvanic couple the generation of low galvanic currents is to be expected because the rate of oxygen reduction, the principal cathodic reaction in aqueous chloride environments, on aluminum is low. Because the galvanic current densities remained small for 700 hours of testing, galvanic coupling between IN-9052 and AA-6061 should not produce deleterious results.

PIT MORPHOLOGIES. SEM examination before removal of corrosion products revealed significant differences between the morphologies of the pits formed on IN-9052 and AA-6061. At 15X, no discernable pits could be seen; however, a number of localized areas of corrosion product build-up were observed. (See Figures 20-21.) At 100X, the localized build-up of corrosion products was more easily seen. Typically for AA-6061, the localized build-up of corrosion products were irregularly shaped and thick; on the other hand, the localized corrosion product build-up on IN-9052 was nearly circular and much smaller in size than observed for AA-6061. (See Figures 22-23.) At 500X, representative localized corrosion products on IN-9052 were more easily seen. (See Figure 24.) In Figure 22, it can be seen that adjacent to the localized build-up of corrosion products on AA-6061 a relatively thick corrosion product layer existed, as indicated by the small area exposed when some of the corrosion product layer broke away, thus showing the underlying surface. At a magnification of 500X, the relative thickness of the corrosion layer was enhanced. (See Figure 25.) An SEM of IN-9052 at the same magnification revealed no such "thick" corrosion product layer; in fact, the original lines of abrasion can be seen in areas adjacent to corrosion product build-up. (See Figure 26.) A comparison of the areas adjacent to the localized corrosion product build-up at 2,000X showed that the corrosion products on AA-6061 were much thicker the observed for IN-9052. (See Figures 27-28.) It can be seen that the original lines of abrasion were still evident on IN-9052, (See Figure 27), but were absent on AA-6061 which indicated that the corrosion products obscured these lines or the abrasion lines on AA-6061 were corrode away. (See Figure 28.) An EDAX scan gave a strong Cl-K_α signal in areas of corrosion product build-up. This observation confirmed that these areas were indeed due to corrosion product formation. In addition, EDAX results taken from areas adjacent to areas of corrosion product build-up indicated the presence of Cl but at a significantly lower concentration. The presence of corrosion product film covering pits is well established and is known to arrest pit growth in some cases. A summary of EDAX results can be seen in Table 3 for two representative pitted areas on both IN-9052 and AA-6061. The amount of Cl found in areas adjacent to localized corrosion product build-up was less for IN-9052 and gave further evidence to support the proposal that attack in these areas was more severe on AA-6061. The presence of a Si-K_α signal on IN-9052 most likely originated from the SiC abrasive paper used in the sample's preparation.

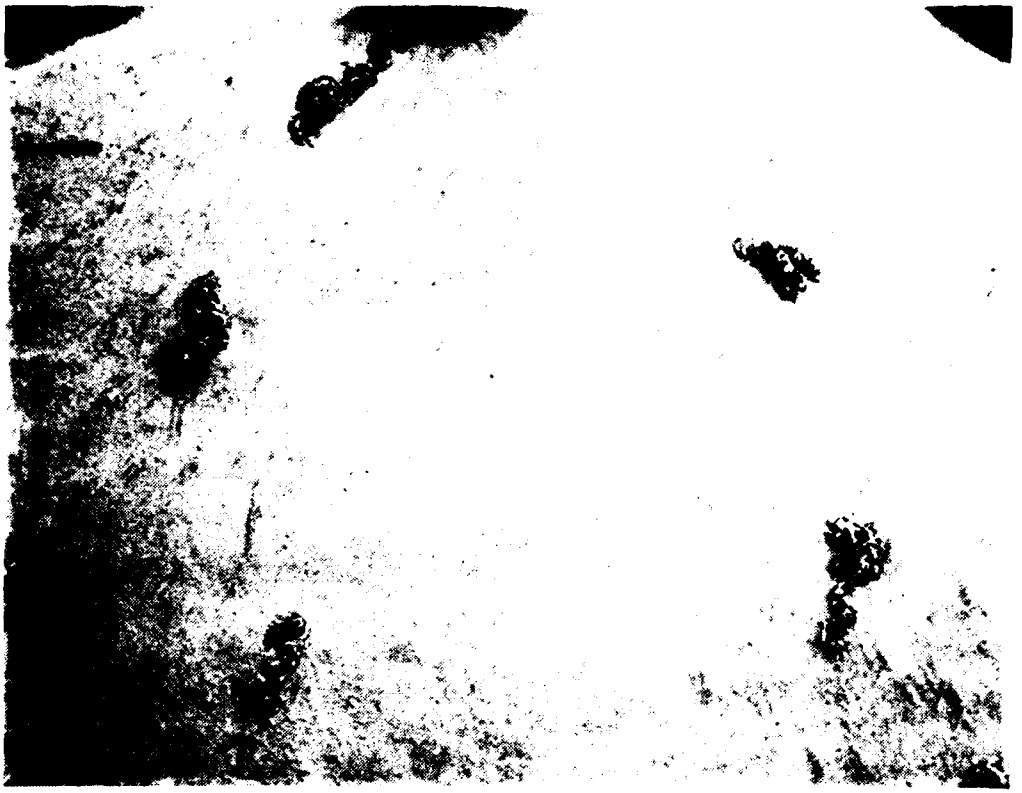

FIGURE 20. SEM PHOTOGRAPH OF LOCALIZED CORROSION PRODUCT BUILD-UP ON AA-6061 EXPOSED TO 3.5% NaCl FOR 5 WEEKS (15X)

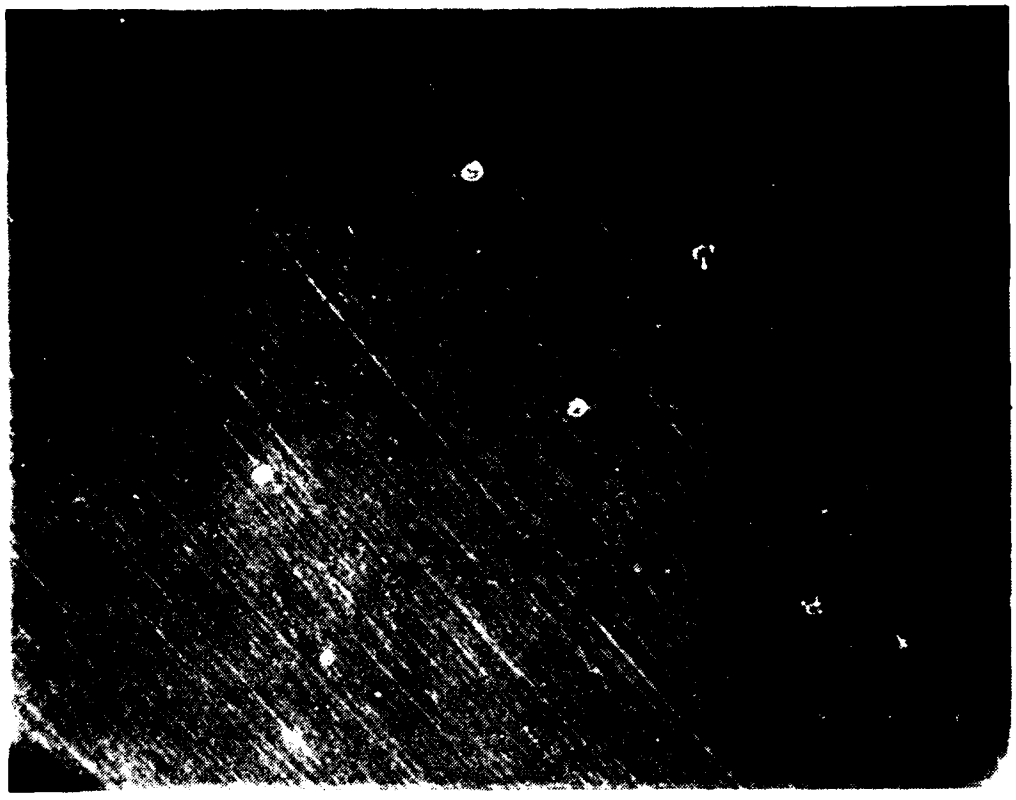

FIGURE 21. SEM PHOTOGRAPH OF LOCALIZED CORROSION PRODUCT BUILD-UP ON IN-9052 EXPOSED TO 3.5% NaCl FOR 5 WEEKS (17X)

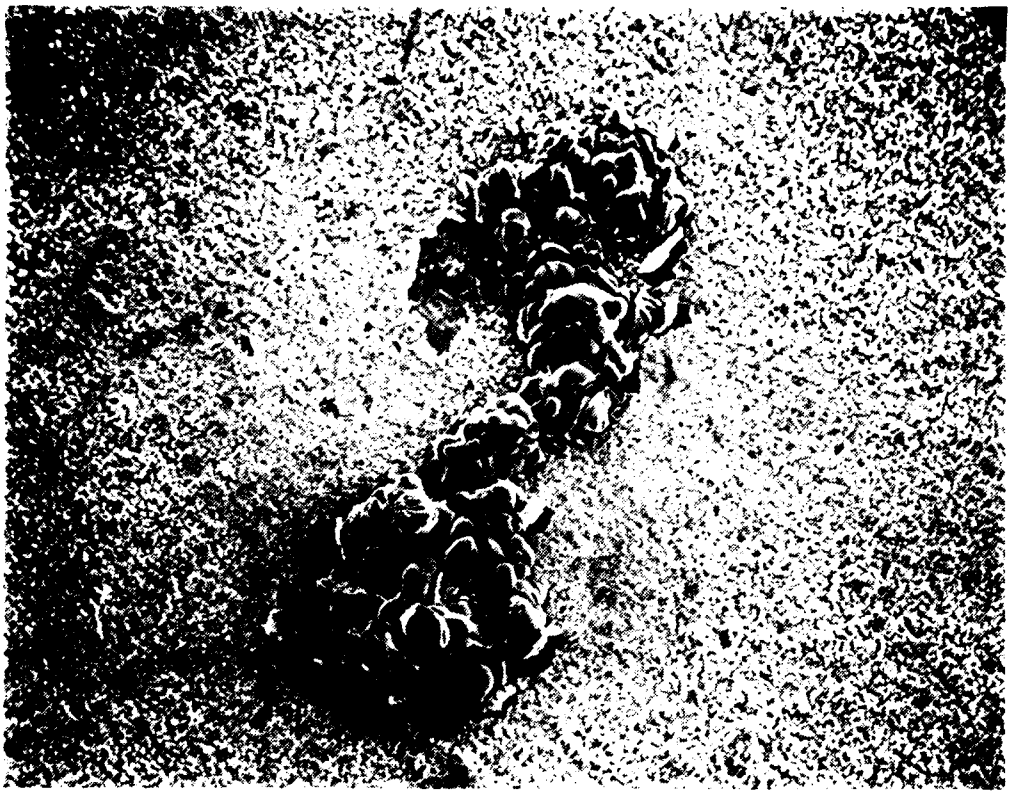

FIGURE 22. SEM PHOTOGRAPH OF IRREGULARLY SHAPED CORROSION PRODUCT BUILD-UP ON AA-6061 (100X)

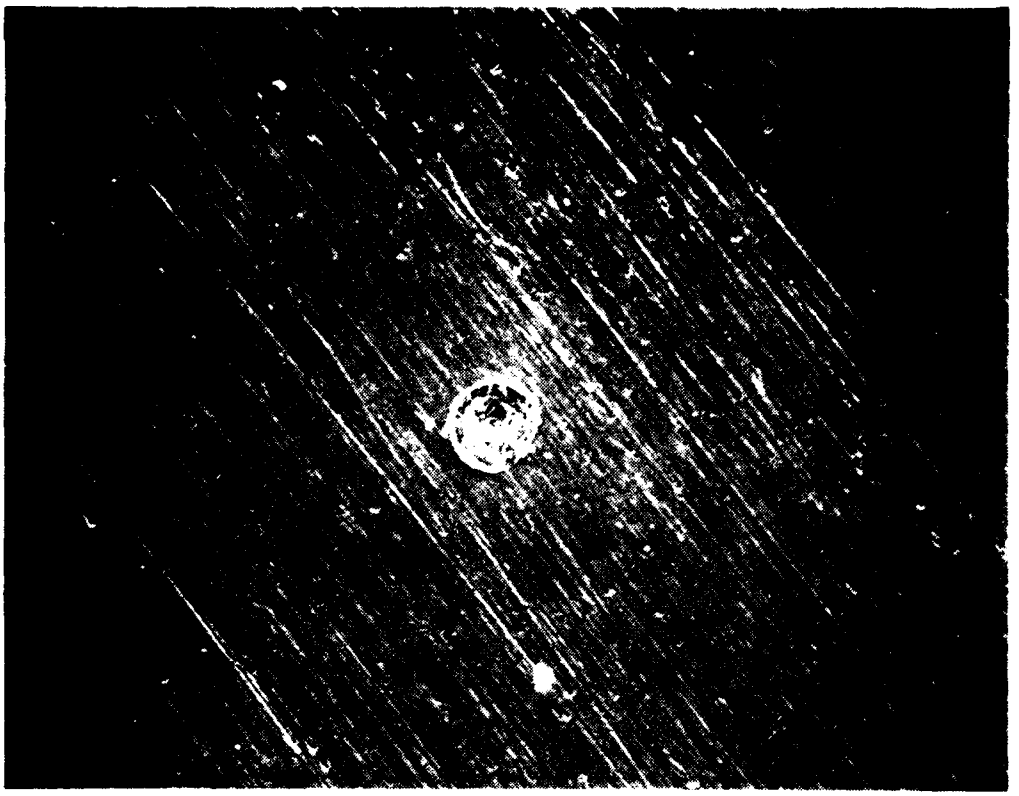

FIGURE 23. SEM PHOTOGRAPH OF ROUNDED CORROSION PRODUCT BUILD-UP ON IN-9052 (100X)

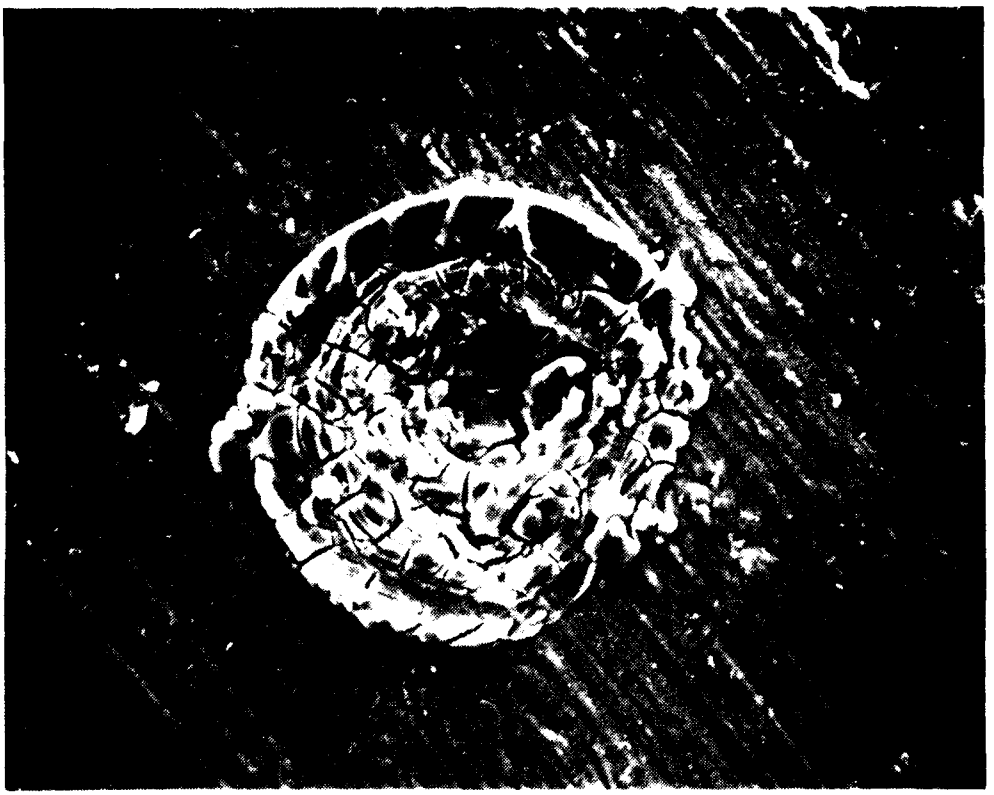

FIGURE 24. HIGH MAGNIFICATION OF ROUNDED CORROSION PRODUCT BUILD-UP ON IN-9052 (500X)

FIGURE 25 CORROSION PRODUCT LAYER ON AA 6061 IN AN AREA ADJACENT TO CORROSION PRODUCT BUILD UP (500X)

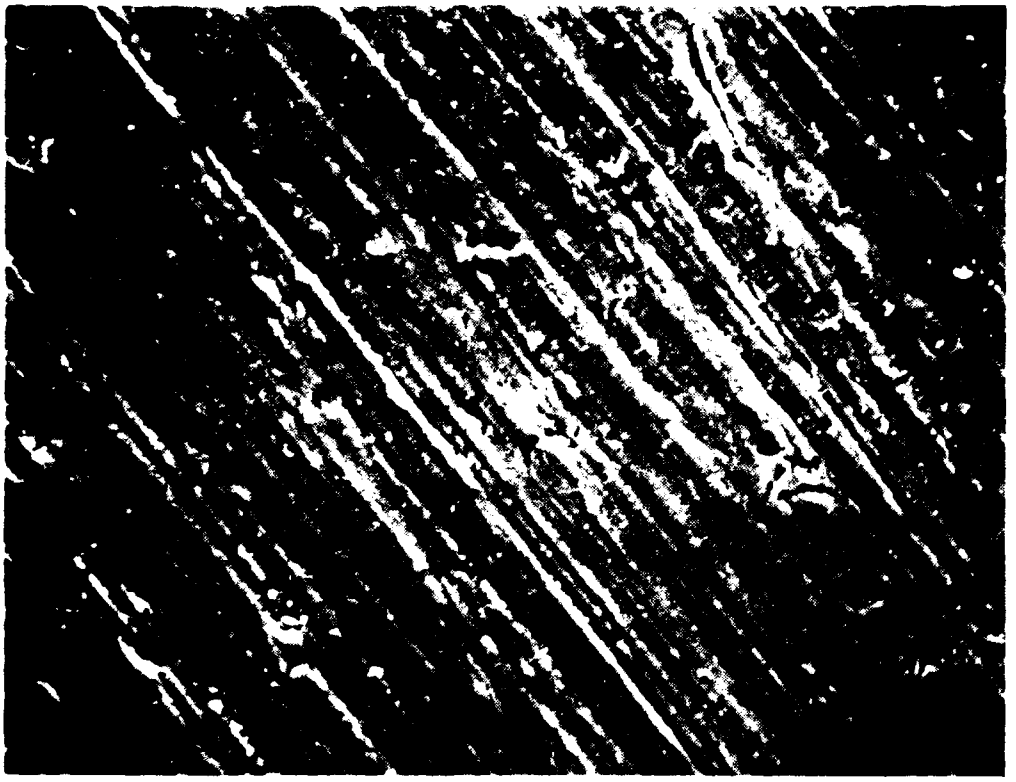

FIGURE 26. AREA ADJACENT TO CORROSION PRODUCT BUILD UP ON IN 9052 (500X)

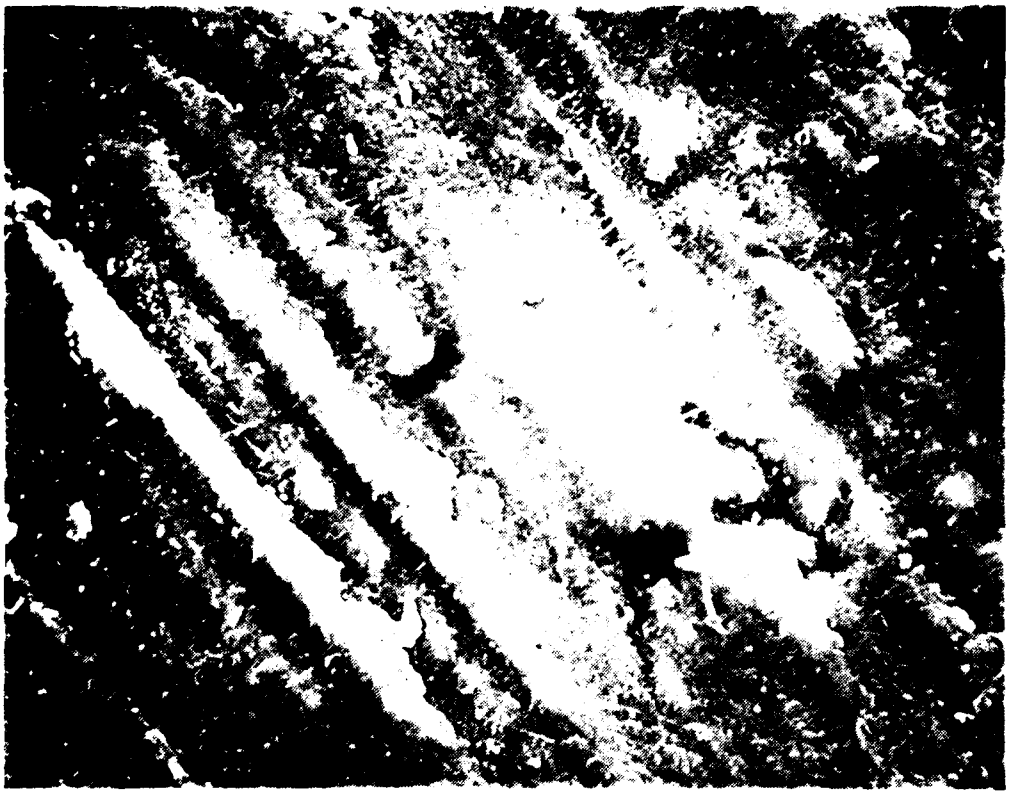

FIGURE 27. HIGH MAGNIFICATION OF AN AREA ADJACENT TO CORROSION PRODUCT BUILD-UP ON IN-9052 (2000X)

FIGURE 28. HIGH MAGNIFICATION OF AN AREA ADJACENT TO CORROSION PRODUCT BUILD-UP ON AA-6061 (2000X)

TABLE 3. SUMMARY OF EDAX RESULTS FOR IN-9052 AND AA-6061 AFTER EXPOSURE TO 3.5% NaCl FOR FIVE WEEKS

Sample	Elements	Concentration Wgt%	Concentration At%
AA-6061:			
Corrosion Products Over Pit # 1	AlK_α	65.95	71.79
	ClK_α	34.05	28.21
Corrosion Film Near Pit # 1	AlK_α	92.22	93.42
	SiK_α	5.13	4.99
	ClK_α	1.04	0.80
	FeK_α	1.61	0.79
Corrosion Products Over Pit # 2	AlK_α	65.97	71.81
	ClK_α	34.03	28.19
Corrosion Film Near Pit # 2	AlK_α	94.56	94.90
	SiK_α	4.73	4.56
	ClK_α	0.70	0.54
IN-9052:			
Corrosion Products Over Pit # 1	MgK_α	1.28	1.59
	AlK_α	53.28	59.68
	ClK_α	45.44	38.73
Corrosion Film Near Pit # 1	MgK_α	4.81	5.31
	AlK_α	92.91	92.59
	SiK_α	2.03	1.94
	ClK_α	0.20	0.15
Corrosion Products Over Pit # 2	MgK_α	1.87	2.22
	AlK_α	69.77	74.63
	SiK_α	0.31	0.32
	ClK_α	28.05	22.83
Corrosion Film Near Pit # 2	MgK_α	4.47	4.94
	AlK_α	94.33	93.96
	SiK_α	0.91	0.87
	ClK_α	0.29	0.22

Removal of corrosion products on AA-6061 revealed a severely pitted surface, an absence of abrasion lines, and large-irregularly shaped deep pits (the large-deep pits were presumably located beneath the areas of corrosion product build-up). A series of SEM photographs, magnified at 75X, 100X, and 500X, of a typical (large) pit on AA-6061 can be seen in Figures 29-31. Conversely, the surface of IN-9052 after removal of corrosion products showed a large number of extremely small-diameter shallow pits with nearly hemispherical shape, the presence of abrasion lines, and large hemispherically shaped pits. The large pits on IN-9052 were much smaller in diameter in comparison to the corresponding large pits on AA-6061, (See Figures 32-34), this was evident when SEM photographs of representative (large) pits on IN-9052 were compared to those described earlier for AA-6061. An SEM photograph obtained at 2,000X for IN-9052 in an area adjacent to a large pit revealed abrasion lines and no signs of additional pitting. (See Figure 35.) On the other hand, a similar SEM photograph for AA-6061 showed an absence of abrasion lines and evidence that several smaller pits were developing. (See Figure 36.)

SEM photographs provided evidence that the pitting mechanisms for IN-9052 and AA-6061 may be different, as indicated by the nature of the pit morphologies. The shape and size of pits found on AA-6061 were typical of ingot metallurgy aluminum alloys; pits were irregularly shaped, deep, and angular in nature, suggesting that pitting occurred along preferred crystallographic planes. Conversely, the pits formed on IN-9052 were small in diameter, shallow, and nearly hemispherical in shape. The hemispherical shape of the pits suggested that pitting did not follow a preferred path. The F.C.C. lattice in IN-9052 is highly strained with low angle boundaries between planes and the formation of pits should be non-directional and round-smooth pits would be expected . Another possible explanation for the small number of pits found on IN-9052 and their characteristic pit shape involves the selective dissolution of Al_4C_3 which is homogeneously dispersed throughout the aluminum matrix (2-3). The carbide dispersoid helps to stabilize the submicron grain size and provide improved strength. However, it is well known that Al_4C_3 is anodic to the aluminum matrix[12] and will react rapidly in aqueous chloride environments; therefore, the selective dissolution of Al_4C_3 by galvanic interaction may result in the formation of rounded pits and also provide sites for pit initiation. It was described previously that the corrosion films on AA-6061 were apparently much thicker than those found on IN-9052, which suggested that the IN-9052 oxide was less reactive, i.e., more protective. With this in mind, following the selective attack of Al_4C_3 the freshly exposed aluminum matrix may rapidly

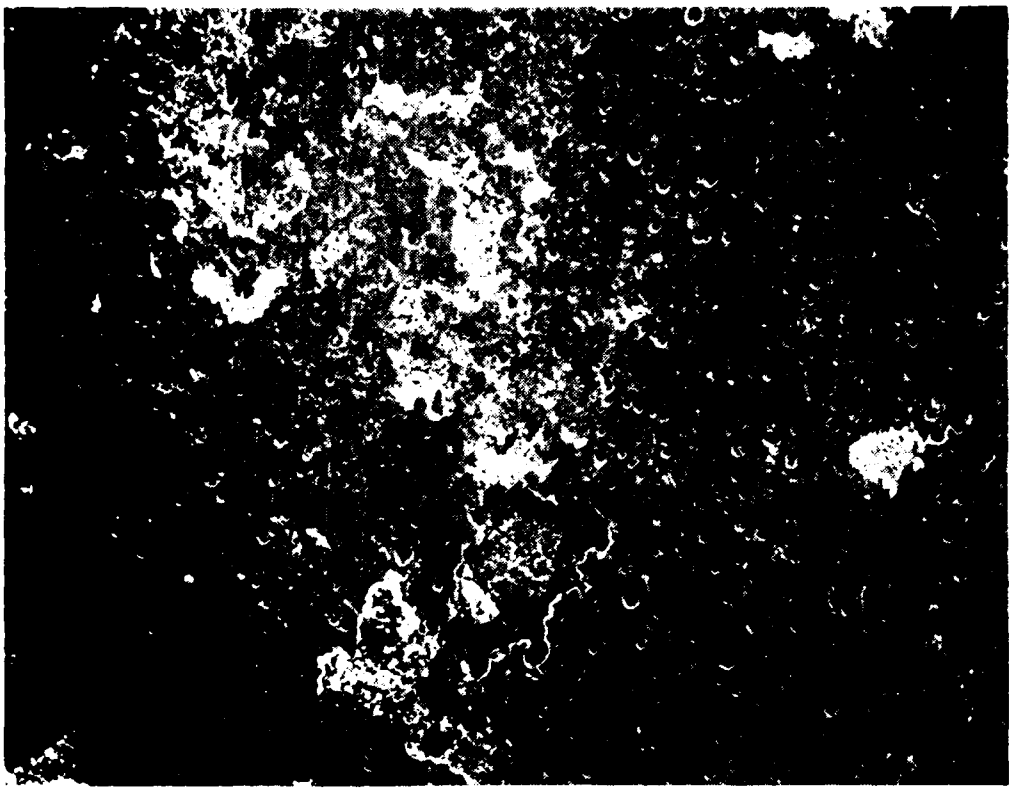

F[illegible] HE[illegible] P[illegible]TED AREA ON AA 6061 AFTER REMOVAL OF CORROSION PRODUCTS (75X)

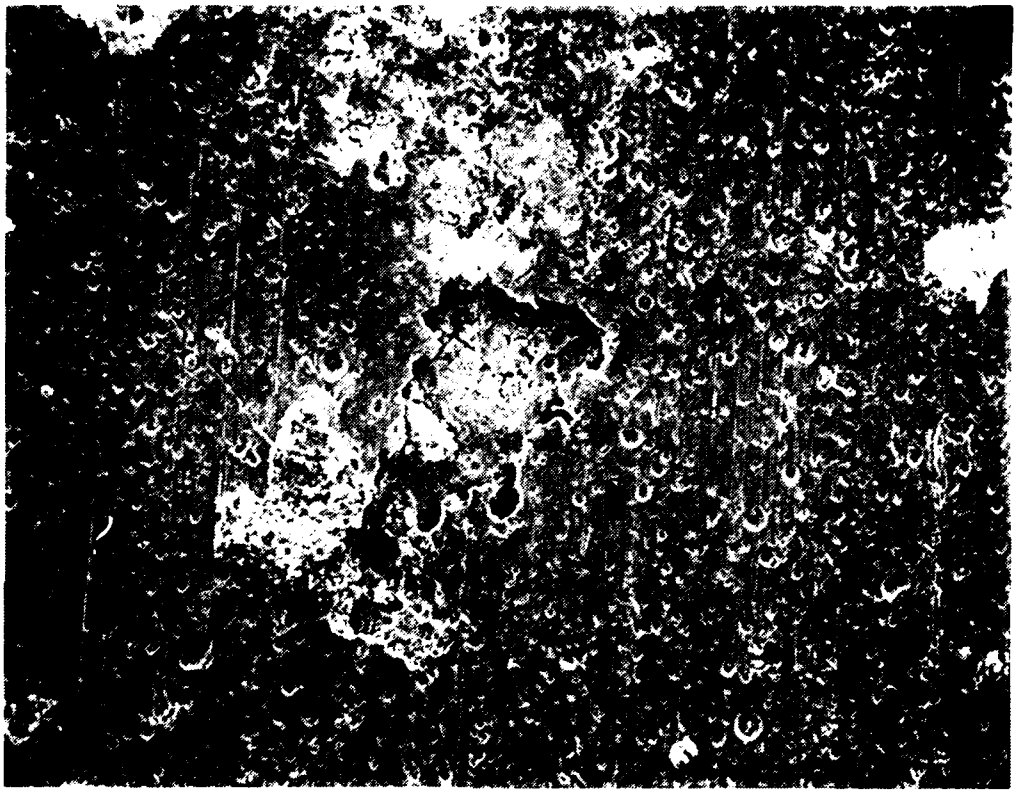

FIGURE 30. PITTED AREA ON AA-6061 AFTER REMOVAL OF CORROSION PRODUCTS (100X)

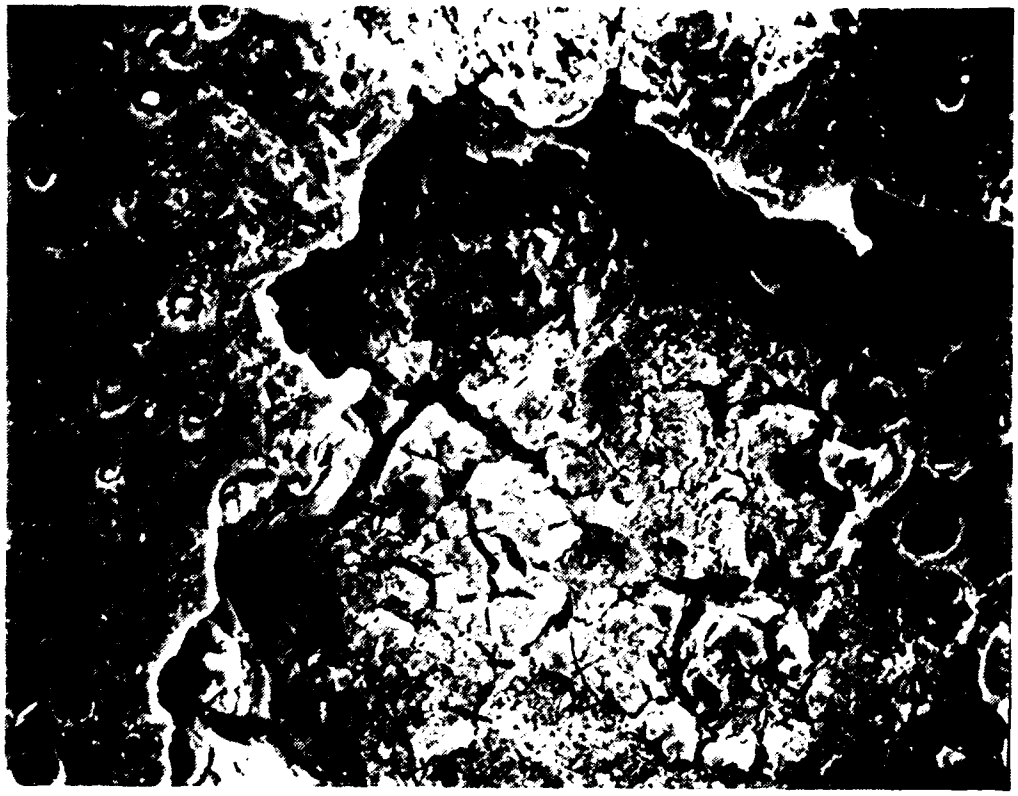

FIGURE 31. PITTED AREA ON AA-6061 AFTER REMOVAL OF CORROSION PRODUCTS (500X)

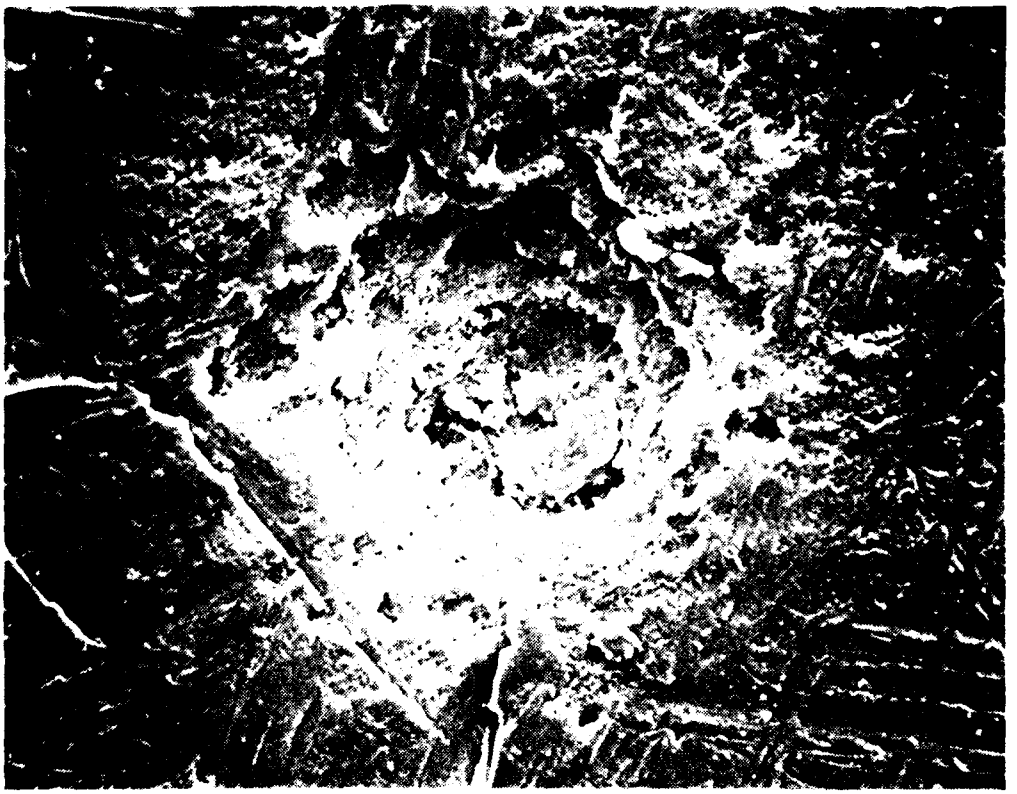

FIGURE 32 REPRESENTATIVE PIT ON IN 9052 AFTER REMOVAL OF CORROSION PRODUCTS (500X)

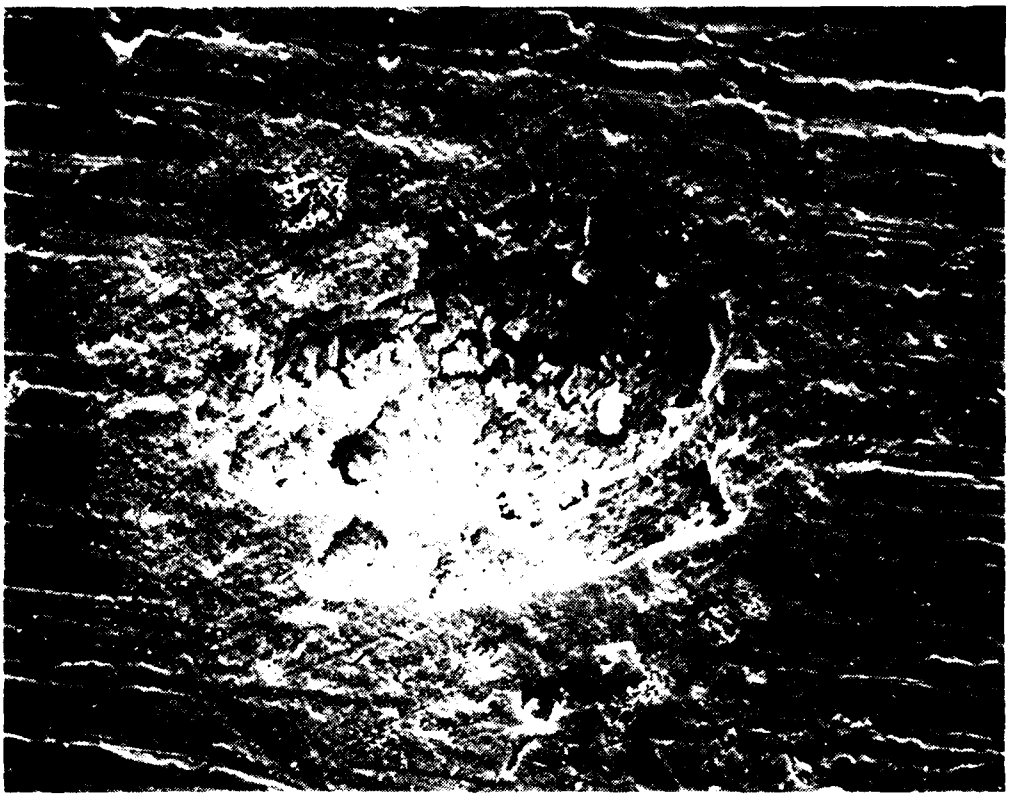

FIGURE 33 REPRESENTATIVE PIT ON IN 9052 AFTER REMOVAL OF CORROSION PRODUCTS (500X)

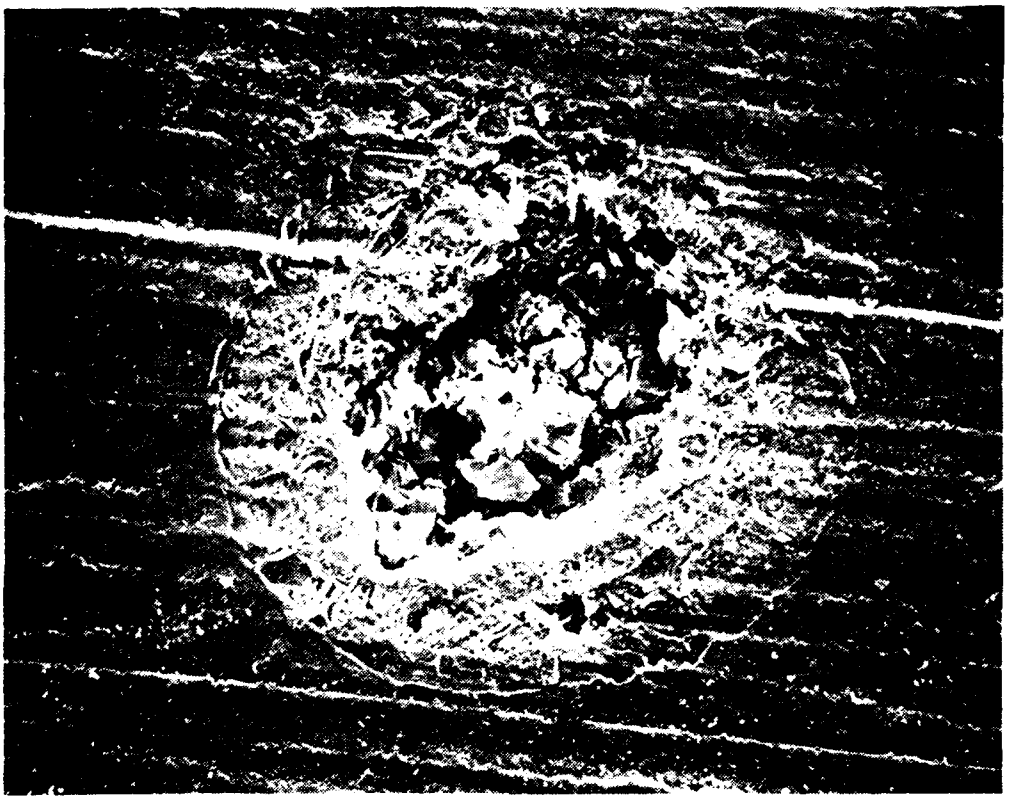

FIGURE 34. REPRESENTATIVE PIT ON IN-9052 AFTER REMOVAL OF CORROSION PRODUCTS (500X)

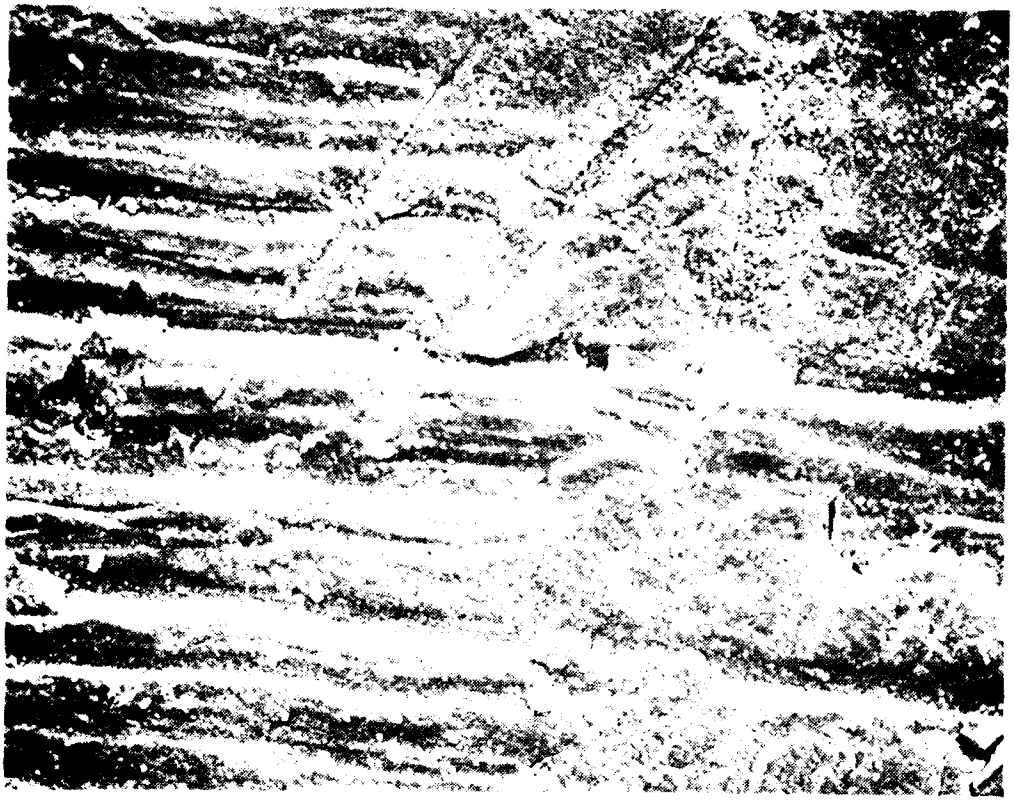

FIGURE 35 AREA ADJACENT TO A PIT ON IN-9052 (2000X)

FIGURE 36. AREA ADJACENT TO A PIT ON AA 6061 (2000X)

passivate, leading to a slower rate of attack. This slower rate of attack would account for the shallowness of the pits formed on IN-9052. Conversely, the developing pit on AA-6061 cannot be repassivated as easily and thus, deeper, larger-diameter pits result which continue to grow until an adherent corrosion product layer builds up over the pit. A schematic of this mechanism can be seen in Figure 37. A similar observation was reported by Metzger and Zahavi[13] for the effect of Al_3Fe on the anodization behavior of Al-1.0Fe in sulfuric acid. Previous studies concluded that Al_3Fe was selectively dissolved,[14] became incorporated into the film,[15] or was anodized at the same rate as the matrix.[16] However, Metzer and Zahavi using SEM and TEM have postulated that Al_3Fe was excavated from the aluminum matrix by a localized pitting and/or crevice mechanism. Localized attack occurred around the Al_3Fe particle eventually lifting it from the matrix. The region immediately adjacent to the Al_3Fe particle was corroded away and the freshly generated surface was simultaneously passivated by the anodizing solution. A schematic of their mechanism can be seen in Figures 38 and 39.

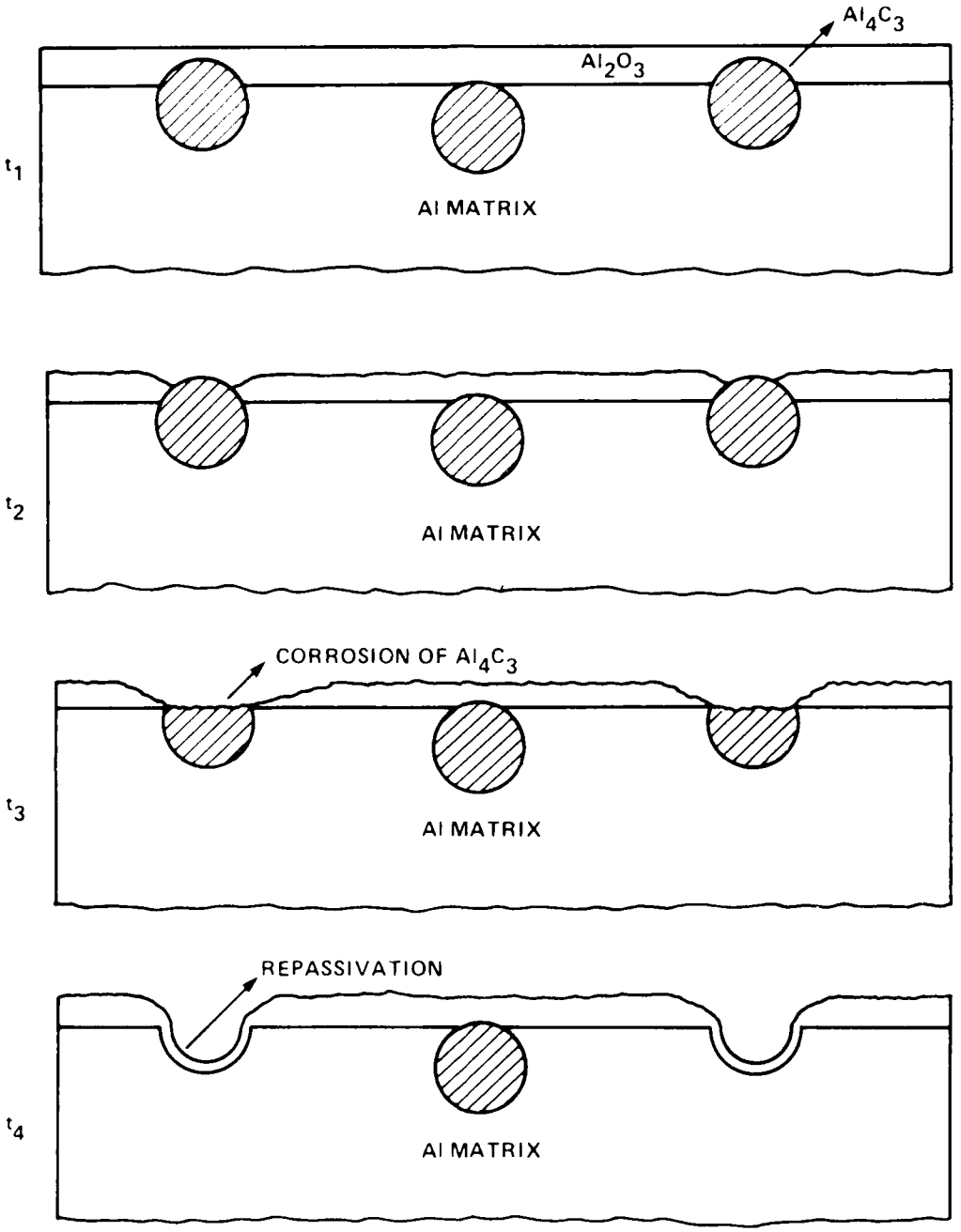

FIGURE 37. SCHEMATIC OF POSSIBLE PIT INITIATION ON IN-9052 EXPOSED TO NaCl ENVIRONMENTS

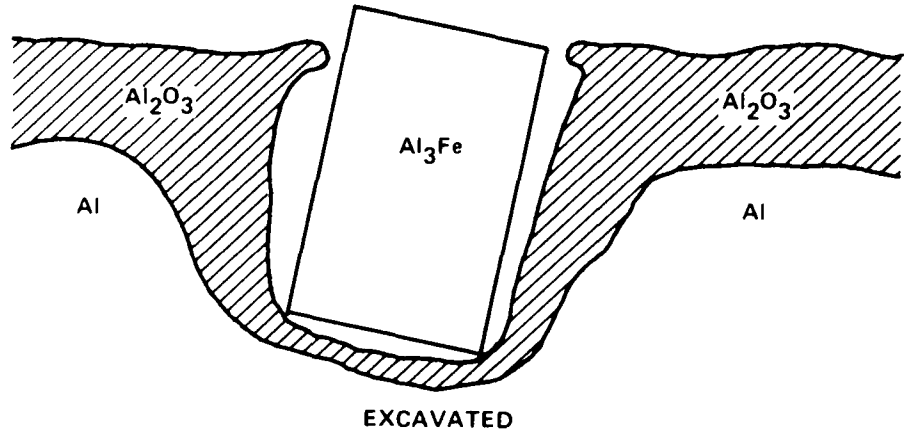

FIGURE 38*. SCHEMATIC OF Al_3Fe PARTICLE EXCAVATED BY PITTING AT ITS MARGINS

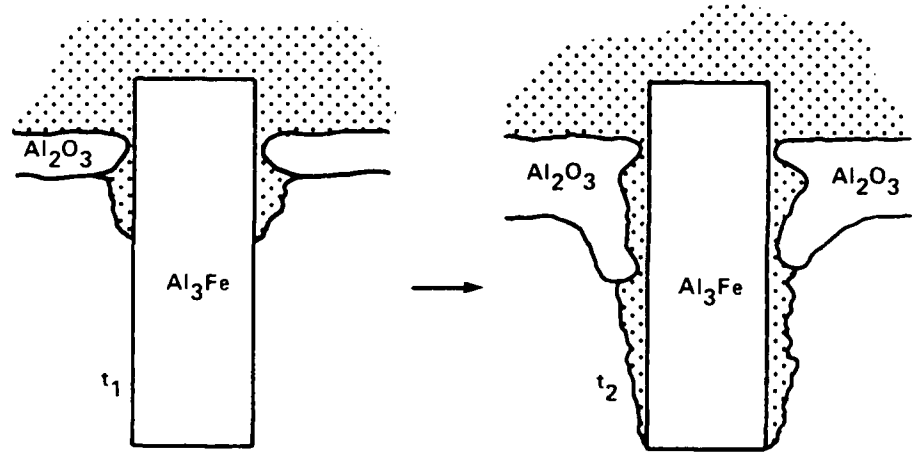

FIGURE 39*. POSSIBLE MECHANISM OF PARTICLE EXCAVATION BY REPEATED BREAKDOWN-PITTING REPAIR

* FROM REFERENCE 13

CHAPTER 5

SUMMARY

1. The uniform corrosion behavior of IN-9052 and AA-6061 exhibited different trends. The corrosion rate of IN-9052 increased initially but eventually decreased to a steady value; however, the corrosion rate of AA-6061 decreased initially but increased, at later times, to a final steady value.

2. Calculated uniform corrosion rates revealed that IN-9052 had a lower rate than AA-6061.

3. SEM examination revealed that a thinner corrosion product layer formed on IN-9052 than on AA-6061. This observation indicated that the oxide film on IN-9052 was more protective, i.e., less reactive. Rp measurements also confirmed this assumption. IN-9052 exhibited much higher Rp values than AA-6061 which indicated that IN-9052 had a lower uniform corrosion rate, i.e., less reactive surface. A final confirmation was obtained from EDAX results which revealed that lower concentration of Cl were found in areas adjacent to pits, i.e., areas of corrosion product build-up.

4. The anodic polarization curves were nearly identical for both IN-9052 and AA-6061, indicating that the anodic dissolution mechanisms were similar.

5. Pitting corrosion was the dominant form of corrosive attack for both IN-9052 and AA-6061.

6. Potentiodynamic cyclic pitting scans showed that both IN-9052 and AA-6061 were susceptible to pitting corrosion. Based on the difference between E_p and E_{corr}, IN-9052 should be somewhat more resistant to pitting.

7. SEM examination of samples exposed to 3.5% NaCl for five weeks revealed that pitting was more severe on AA-6061; pits were deeper and larger than those observed on IN-9052. In addition, the pits on IN-9052 were rounded while those on AA-6061 were irregularly shaped.

8. It was proposed that pit initiation on IN-9052 occurred on and/or around Al_4C_3 particles, thus, producing rounded pits in areas previously occupied by Al_4C_3. Once the Al_4C_3 particle was dissolved or removed, the resulting cavity (pit) repassivated and pit propagation slowed, i.e., yielding shallow pits.

9. Galvanic coupling of SS-316 to IN-9052 appeared to be worse than AA-6061 coupled to SS-316. The galvanic current dersity for the SS-316/AA-6061 couple remained small for the duration of the test period; although the initial galvanic current densities were similarly small for the SS-316/IN-9052 couple, at later times, the galvanic current density increased. The observed increase in the galvanic current density was attributed to the presence of crevice corrosion.

10. Although IN-9052 behaved as the anode when coupled to AA-6061, the generated galvanic currents were small. Because the galvanic currents remained small for the duration of the test, IN-9052 and AA-6061 were apparently compatible with little or no accelerated corrosion.

REFERENCES

1. Gilman, P.S. and Donachie, S.J., Ann. Rev. Matr. Sci., Vol. 13, 1983, p. 279.

2. Schelleng, R.D. and Donachie, S.J., Metal Powder Report, Vol. 38, No. 10, 1983, p. 575.

3. Bridges, P.J., "Aluminum-Base Alloy Made by Mechanical Alloying," PM Aerospace Materials, Vol. I, (Berne, Switzerland, 12-14 Nov, 1984), paper #30.

4. Scully, J.C., The Fundamentals of Corrosion (Oxford: Pergamon Press, 1975).

5. Fontana, M.G. and Greene, N.D., Corrosion Engineering, (New York: McGraw-Hill Co., 1978).

6. Erich, D.L. and Donachie, S.J., Metal Progress, Feb 1982 p. 22.

7. Shaw, W.J.D., Corrosion, Vol. 42, No. 9, 1986, p. 554.

8. Stern, M. and Geary, A.L., Electrochemical Society Journal, Vol. 104, 1957, p. 56.

9. Mansfeld, F., Corrosion, Vol. 27, No. 10, 1971, p. 436.

10. Mansfeld, F., Corrosion, Vol. 29, No. 10, 1973, p. 403.

11. Mansfeld, F., Corrosion Science, Vol. 13, 1973, p. 651.

12. Metzger, M. and Fishman, S.G., Ind. Eng. Chem. Product Research and Devlopment, Vol. 22, No. 2, 1983, p. 296.

13. Metzger, M. and Zahavi, J.,"Film Growth and Breakdown Processes on Aluminum Observed by Electron Microscopy," in Passivity of Metals, Ed., Frankenthal, R.P. and Kruger, J. (Princeton, NJ: The Electrochemical Society, Inc., 1978), p. 960.

14. Keller, F., Wilcox, G.W., Tosterund, M., and Slunder, C.J., Metals and Alloys, Vol. 10, 1939, p. 219.

15. Wood, G.C. and Brock, A.J., Trans. Inst. Metal Finish., Vol. 44, 1966, p. 189.

16. Cote, J., Howlett, E.E., Wheller, M.J., and Lamb, H.J., Plating, Vol. 56, 1969, p. 386.

DISTRIBUTION

	Copies
Office of Naval Research Attn: S. Fishman, Code 1131 800 N. Quincy Street Arlington, VA 22217	2
Office of Deputy Undersecretary of Defense Attn: J. Persh Staff Specialist for Materials Washington, DC 20301	1
Defense Advanced Research Attn: P. Parrish 1400 Wilson Blvd. Arlington, VA 22209	1
Naval Ocean Systems Command Attn: P. D. Burke, Code 903 J. Maltby, Code 932 San Diego, CA 92152	1 1
Naval Sea Ssytems Command Attn: S. Rodgers, SEA 05M1 H. Bliele, SEA 05M1 Washington, DC 20362	1 1
Naval Air Development Center Attn: V. Agarwala, Code 6062 J. Thompson, Code 6062 Warminister, PA 18974-5000	4
Commanding Officer Attn: B. Sanoman Naval Underwater Systems Center Newport, R. I. 02840	1
Department of the Army Attn: A. Levitt DRXMR-MMC, Bldg. 39 Watertown, MA 02712	1
Naval Research Laboratory Attn: R. Crowe, Code 6372 E. McCafferty P. Trzaskoma P. Natishan Washington, DC 20375	1 1 1 1
Naval Material Command Attn: J. J. Kelly, Code 0725 A. J. Sedriks, Code 431 Office of Navy Technology Washington, DC 20360	1 1
Defense Technical Information Center Cameron Station Alexandria, VA 22314	12
Library of Congress Cameron Station Alexandria, VA 22315	4
David Taylor Naval Ship Research and Development Center Attn: T. Morton, Code 2813 H. Hack, Code 2813 J. Scully, Code 2813	1 1 1
Vance Saige PMS 400C52 NC210S18 2521 Jeff-Davis Highway Arlington, VA 22202	1

DISTRIBUTION (Cont.)

	Copies
Naval Ship Systems Engineering Station Attn: N. Clayton, Code 053B	1
NUCPWPSCH Attn: Paul A. Stone NTC, Orlando R30 Orlando, FL	1
Novamet Attn: B. Schelling 681 Laulins Road Wycoff, NJ 07481	2

Internal Distribution:		Copies
R33	(Le)	1
R33	(McIntyre)	10
R33	(Larrick)	1
R33	(Dacres)	1
R32	(Garrett)	10
R32	(Tydings)	5
R32	(Hoover)	1
R32	(Sutula)	1
R35	(Musselman)	1
R34		1
R34	(Norr)	1
U32	(Woodfield)	1
U10		1
U11D	(Johnson)	2
U11	(Bullock)	2
U11	(Ruben)	2
U07		1
U08		1
G20		1
G30		1
E231		2
E232		15
E342	(GIDEP)	1

END

10-87

DTIC